Supporting Information

Aggregation-induced emission of cyclometalated rhodium(III) and iridium(III) phenylpyridine complexes with ancillary 1,3-diketones

Marina A. Kiseleva, Andrei V. Churakov, Ilya V. Taydakov, Mikhail T. Metlin, Sergey A. Kozyukhin and Stanislav I. Bezzubov

1. Experimental Section

Materials and methods

All commercially available reagents were at least reagent grade and used without further purification. Solvents were distilled and dried according to standard procedures. Preparation of rhodium(III) and iridium(III) complexes was carried out under dry argon. Purification and other manipulations with complexes were performed in air.

^{1}H NMR spectra were acquired at 25 °C on a Bruker Avance 400 instrument and chemical shifts were reported in ppm referenced to residual solvent signals. High resolution and accurate mass measurements were carried out using a BrukermicroTOF-Q^{TM} APPI-TOF (Atmospheric Pressure PhotoIonization / Time of Flight) spectrometer. Electronic absorption spectra were measured on an OKB Spectr SF-2000 spectrophotometer. Luminescence measurements of the complexes in solution were performed on a Perkin-Elmer LS-55 spectrometer. For solids and suspensions, luminescence measurements were performed on a Horiba Fluorolog QM spectrometer equipped with a 75 W xenon arc lamp as the excitation source for steady state experiments, 150 W xenon flash lamp and pulse DeltaLED sources for kinetic measurements. An R-13456 photomultiplier was used as a detector. The quantum yield measurements were carried out on solid samples with a Spectralone-covered G8 integration sphere (GMP SA, Switzerland) according to the absolute method of Wrighton [1-3]. Each sample was measured several times under slightly different experimental conditions. The estimated error for quantum yields was ± 10%. Powdered samples were placed in quartz tubes (4 mm o.d.), flushed with dry nitrogen and sealed. These tubes were used for both luminescent and quantum yield measurements. An Econix-Expert Ltd Ecotest-VA polarograph was used for electrochemical measurements with a glassy carbon working electrode, platinum counter electrode, and saturated Ag/AgCl reference electrode. Polarographic curves were recorded in Ar-saturated acetonitrile with 0.1 M (n-Bu_4N)PF_6 at a scan rate of 100 mV/s. Ferrocene was used as an external standard prior to and after measurements. Scanning electron microscopic (SEM) imaging of the precipitated complexes was performed using a Helios G4CX FEI (Thermo Fisher Scientific Inc., Waltham, MA, USA).

Synthesis

Preparation of cyclometalated Ir(III) and Rh(III) chloride precursors:

$IrCl_3 \cdot 3H_2O$ (0.055 g, 0.156 mmol) or $RhCl_3 \cdot 3H_2O$ (0.055 g, 0.209 mmol) and 2-phenylpyridine (0.390 mmol or 0.523 mmol, respectively) were refluxed for 18 h in 2-

ethoxyethanol (15 mL). After cooling to room temperature, the resulting yellow solids were collected, washed with ethanol, ether, dissolved in CH_2Cl_2, purified by recrystallization from CH_2Cl_2/petroleum ether and dried in vacuo.

$[Ir(ppy)_2Cl]_2$: yellow – orange powder, yield 80%.

$[Rh(ppy)_2Cl]_2$: pale yellow powder, yield 76%.

^{1}H NMR (400 MHz, $CDCl_3$) δ 9.22 (d, J = 5.5 Hz, 4H), 7.89 – 7.79 (m, 8H), 7.57 – 7.54 (m, 4H), 6.85 – 6.76 (m, 8H), 6.65 (t, J = 7.5 Hz, 4H), 5.95 (d, J = 7.8 Hz, 4H).

M.p. >310 °C.

Complexes **Rh1** – **Rh4** and **Ir1** – **Ir4** were obtained according to a general procedure:

Cyclometalated Ir(III) or Rh(III) chloride (1 mmol), corresponding diketone (2.5 mmol) and K_2CO_3 (10 mmol) were mixed in dry acetonitrile (5 ml) and refluxed for 16-20 h in darkness. The precipitate formed (from pale yellow to dark orange) was collected by filtration, washed with water, dissolved in CH_2Cl_2, purified by recrystallization from CH_2Cl_2/petroleum ether and dried in vacuo.

$Rh(ppy)_2(dbm)$ (Rh1): yellow powder, yield 80%.

^{1}H NMR (400 MHz, $CDCl_3$) δ 8.61 – 8.57 (m, 2H), 7.87 (d, J = 8.0 Hz, 2H), 7.82 – 7.77 (m, 6H), 7.64 (dd, J_1 = 7.7, J_2 = 1.3 Hz, 2H), 7.39 – 7.34 (m, 2H), 7.33 – 7.28 (m, 4H), 7.13 – 7.08 (m, 2H), 6.95 (td, J_1 = 7.5, J_2 = 1.2 Hz, 2H), 6.83 (td, J_1 = 7.5, J_2 = 1.4 Hz, 2H), 6.56 (s, 1H), 6.41 (d, J = 7.6 Hz, 2H).

HRMS (API) m/z: $[M+H]^+$ Calcd for $C_{37}H_{28}N_2O_2Rh$ 635.1201; Found 635.1194.

M.p. >310 °C.

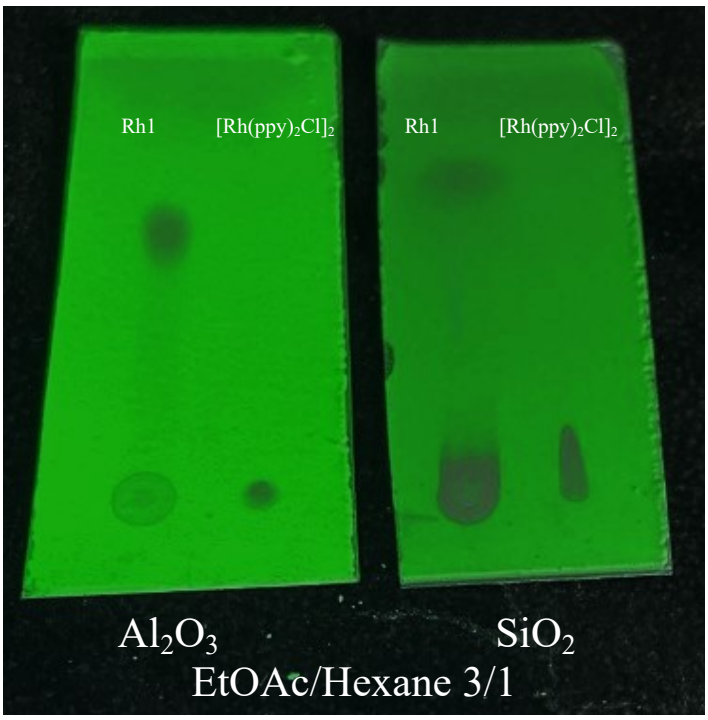

Rh(ppy)$_2$(bza) (Rh2): pale yellow powder, yield 85%.

^{1}NMR (400 MHz, $CDCl_3$) δ 8.57 (d, *J* = 5.5 Hz, 1H), 8.53 (d, *J* = 5.5 Hz, 1H), 7.90 – 7.80 (m, 4H), 7.72 – 7.68 (m, 2H), 7.64 – 7.59 (m, 2H), 7.35 – 7.30 (m, 1H), 7.26 – 7.23 (m, 2H), 7.19 – 7.11 (m, 2H), 6.95 – 6.88 (m, 2H), 6.82 – 6.77 (m, 2H), 6.38 – 6.32 (m, 2H), 5.89 (s, 1H), 2.02 (s, 3H).

HRMS (API) m/z: $[M]^+$ Calcd for $C_{32}H_{25}N_2O_2Rh$ 572.0971; Found 572.0963.

M.p. 279-280 °C.

Rh(ppy)$_2$(tfbza) (Rh3): yellow powder, yield 92%.

^{1}H NMR (400 MHz, $CDCl_3$) δ 8.52 (d, *J* = 5.6 Hz, 1H), 8.41 (d, *J* = 5.6 Hz, 1H), 7.91 – 7.83 (m, 4H), 7.77 – 7.73 (m, 2H), 7.64 – 7.60 (m, 2H), 7.45 – 7.39 (m, 1H), 7.34 – 7.29 (m, 2H), 7.23 – 7.18 (m, 1H), 7.17 – 7.12 (m, 1H), 6.99 – 6.91 (m, 2H), 6.85 – 6.77 (m, 2H), 6.36 (d, *J* = 7.7 Hz, 1H), 6.32 – 6.28 (m, 2H).

HRMS (API) m/z: $[M]^+$ Calcd for $C_{32}H_{22}F_3N_2O_2Rh$ 626.0688; Found 626.0682.

M.p. 290-291 °C.

Rh(ppy)$_2$(tta) (Rh4): yellow powder, yield 84%.

^{1}H NMR (400 MHz, $CDCl_3$) δ 8.53 – 8.50 (m, 1H), 8.47 – 8.43 (m, 1H), 7.90 – 7.83 (m, 4H), 7.63 – 7.59 (m, 2H), 7.56 (dd, J_1 = 3.8, J_2 = 1.1 Hz, 1H), 7.40 (dd, J_1 = 5.0, J_2 = 1.1 Hz, 1H),

7.23 – 7.19 (m, 1H), 7.19 – 7.14 (m, 1H), 7.01 – 6.90 (m, 3H), 6.84 – 6.76 (m, 2H), 6.34 (d, J = 7.6 Hz, 1H), 6.28 (d, J = 7.6 Hz, 1H), 6.15 (s, 1H).

HRMS (API) m/z: $[M]^+$ Calcd for $C_{30}H_{20}F_3N_2O_2RhS$ 632.0253; Found 632.0243.

M.p. >310 °C.

Ir(ppy)$_2$(dbm) (Ir1): light orange powder, yield 65%.

^{1}H NMR (400 MHz, $CDCl_3$) δ 8.60 (d, J = 5.0 Hz, 2H), 7.87 (d, J = 8.1 Hz, 2H), 7.84 – 7.79 (m, 4H), 7.72 – 7.66 (m, 2H), 7.62 – 7.58 (m, 2H), 7.43 – 7.38 (m, 2H), 7.33 – 7.27 (m, 4H), 7.08 – 7.02 (m, 2H), 6.89 – 6.84 (m, 2H), 6.75 (td, J_1 = 7.4, J_2 = 1.2 Hz, 2H), 6.59 (s, 1H), 6.41 – 6.34 (m, 2H).

HRMS (API) m/z: $[M]^+$ Calcd for $C_{37}H_{27}N_2O_2Ir$ 724.1699; Found 724.1700.

M.p. 302-303 °C.

Ir(ppy)$_2$(bza) (Ir2): dark yellow powder, yield 86%.

^{1}H NMR (400 MHz, $CDCl_3$) δ 8.58 (d, J = 5.6 Hz, 1H), 8.54 (d, J = 5.5 Hz, 1H), 7.86 (t, J = 8.9 Hz, 2H), 7.75 – 7.68 (m, 4H), 7.60 – 7.56 (m, 2H), 7.39 – 7.33 (m, 1H), 7.27 – 7.23 (m, 2H), 7.13 – 7.05 (m, 2H), 6.86 – 6.80 (m, 2H), 6.75 – 6.69 (m, 2H), 6.37 – 6.28 (m, 2H), 5.90 (s, 1H), 1.92 (s, 3H).

HRMS (API) m/z: $[M]^+$ Calcd for $C_{32}H_{25}N_2O_2Ir$ 662.1542; Found 662.1540.

M.p. 274-274 °C.

Ir(ppy)$_2$(tfbza) (Ir3): orange powder, yield 89%.

^{1}H NMR (400 MHz, $CDCl_3$) δ 8.52 (d, J = 5.5 Hz, 1H), 8.41 (d, J = 5.7 Hz, 1H), 7.88 (t, J = 8.2 Hz, 2H), 7.79 – 7.73 (m, 4H), 7.60 – 7.56 (m, 2H), 7.48 (t, J = 7.5 Hz, 1H), 7.31 (t, J = 7.8 Hz, 2H), 7.18 – 7.14 (m, 1H), 7.12 – 7.07 (m, 1H), 6.91 – 6.83 (m, 2H), 6.77 – 6.70 (m, 2H), 6.34 – 6.30 (m, 2H), 6.27 (d, J = 7.6 Hz, 1H).

HRMS (API) m/z: $[M]^+$ Calcd for $C_{32}H_{22}F_3N_2O_2Ir$ 716.1259; Found 716.1257.

M.p. 298-299 °C.

Ir(ppy)$_2$(tta) (Ir4): dark orange - red powder, yield 74%.

^{1}H NMR (400 MHz, $CDCl_3$) δ 8.51 (d, J = 5.7 Hz, 1H), 8.46 (d, J = 5.7 Hz, 1H), 7.87 (t, J = 8.4 Hz, 2H), 7.79 – 7.73 (m, 2H), 7.64 – 7.62 (m, 1H), 7.57 (d, J = 8.0 Hz, 2H), 7.49 – 7.47 (m,

1H), 7.19 – 7.14 (m, 1H), 7.14 – 7.10 (m, 1H), 7.02 – 6.98 (m, 1H), 6.89 – 6.82 (m, 2H), 6.76 – 6.69 (m, 2H), 6.31 – 6.28 (m, 1H), 6.26 – 6.23 (m, 1H), 6.16 (s, 1H).

HRMS (API) m/z: $[M]^+$ Calcd for $C_{30}H_{20}F_3N_2O_2IrS$ 722.0821; Found 722.0822.

M.p. >310 °C.

2. NMR spectroscopy data and high-resolution mass-spectrometry data

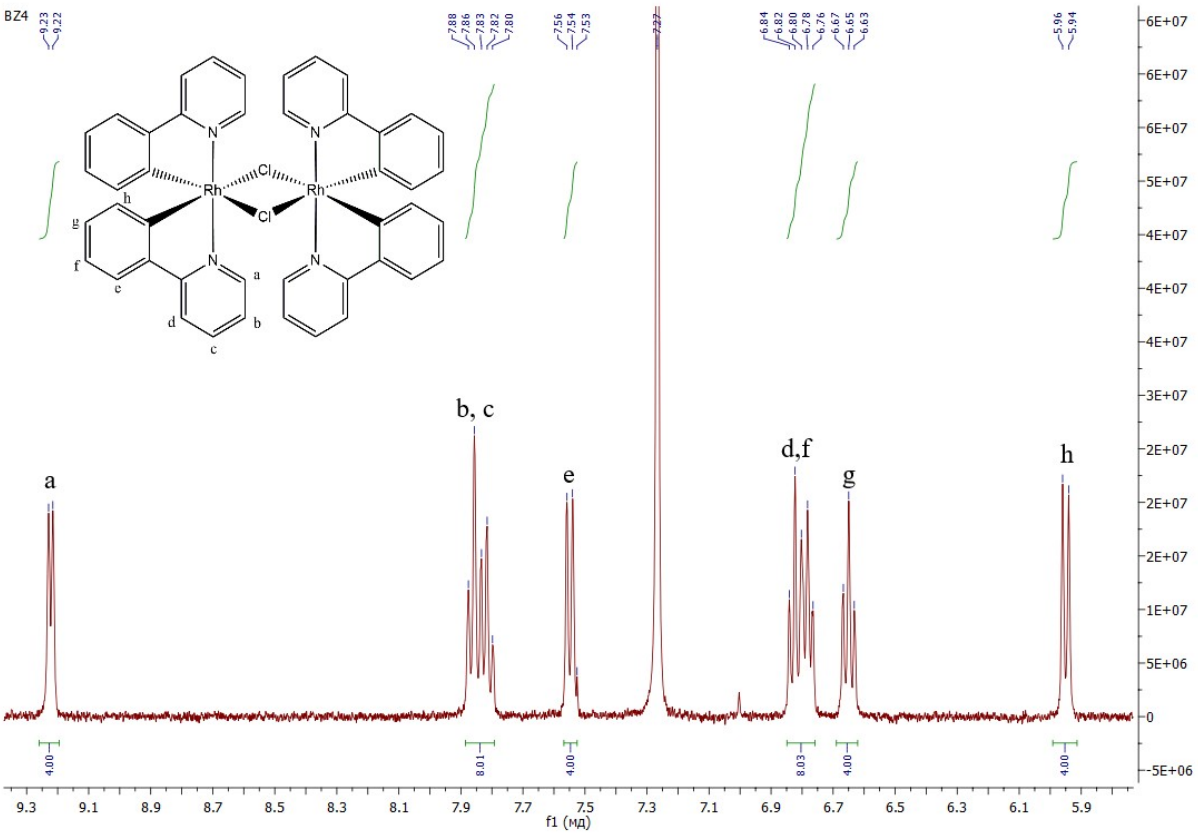

Figure S1. ^{1}H NMR spectrum of $[Rh(ppy)_2Cl]_2$ (400 MHz, 298K, $CDCl_3$).

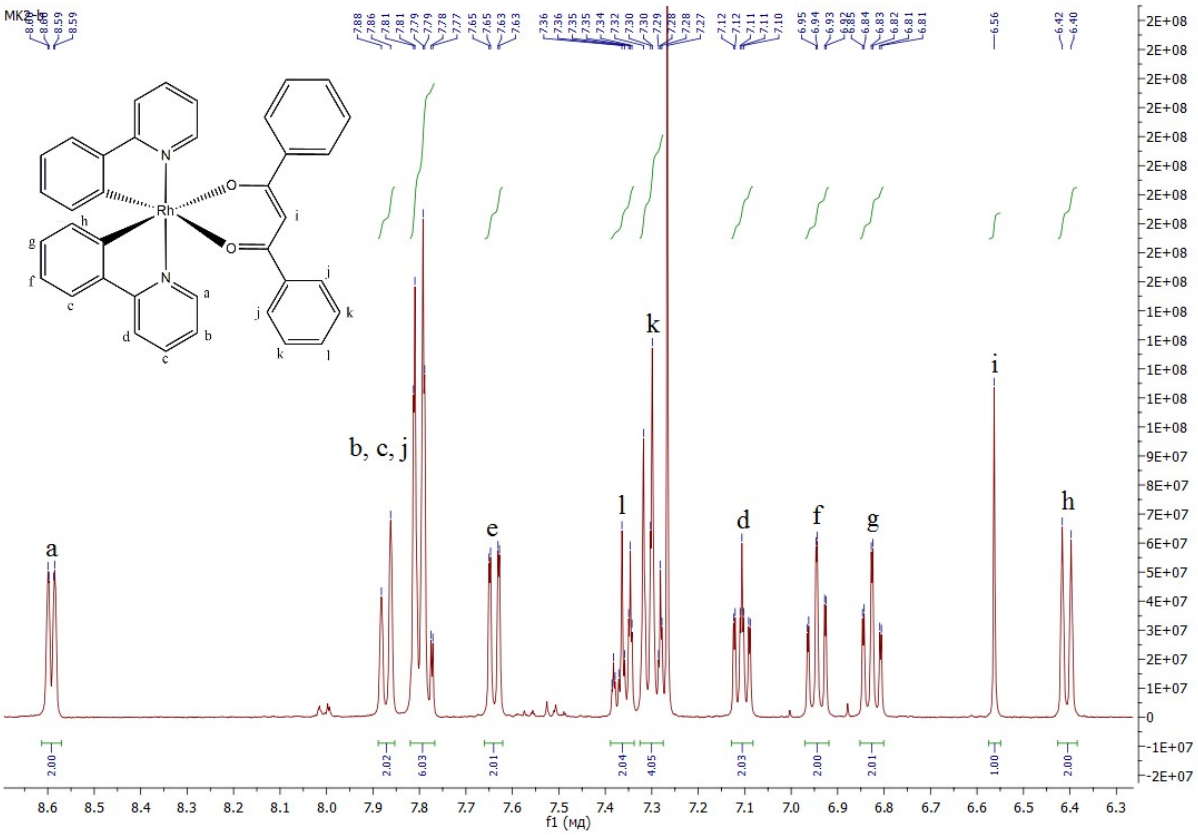

Figure S2. ^{1}H NMR spectrum of **Rh1** (400 MHz, 298K, $CDCl_3$).

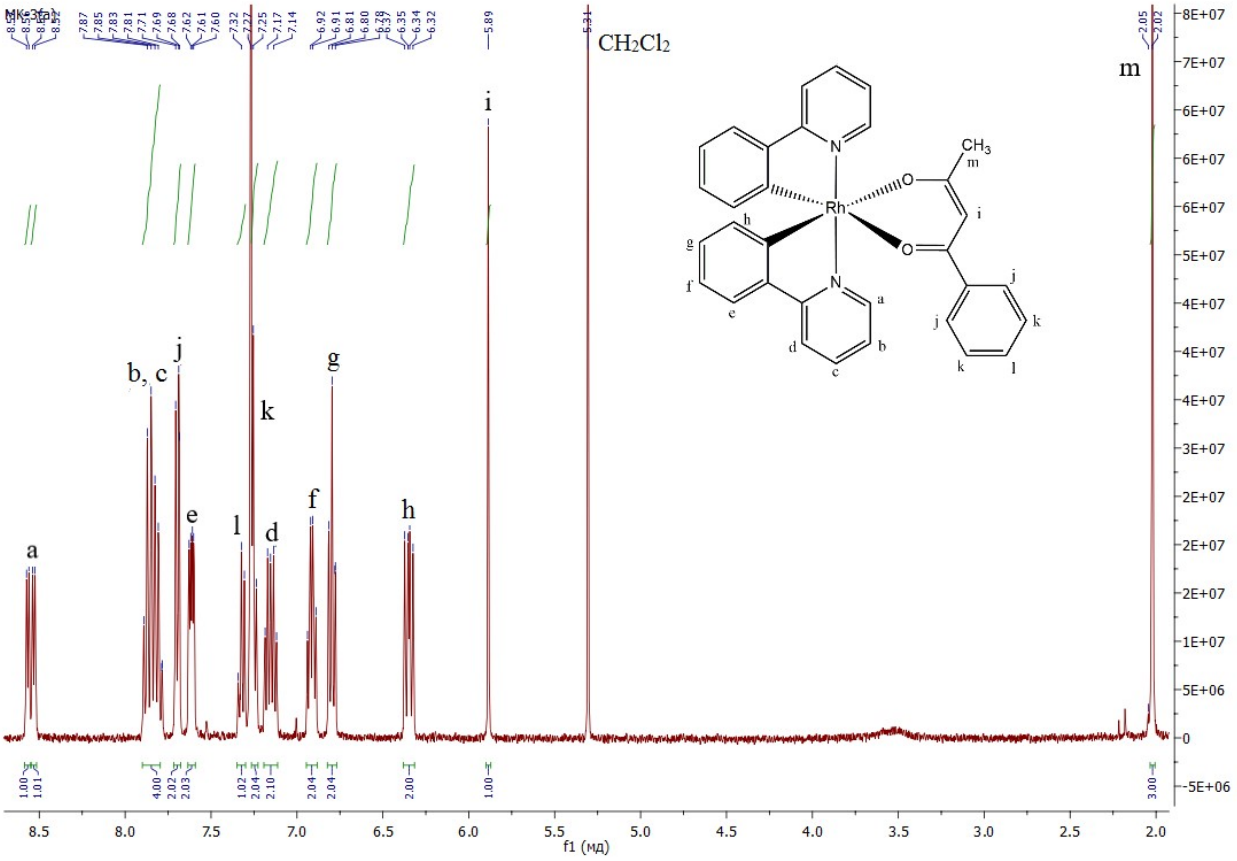

Figure S3. ^{1}H NMR spectrum of **Rh2** (400 MHz, 298K, $CDCl_3$).

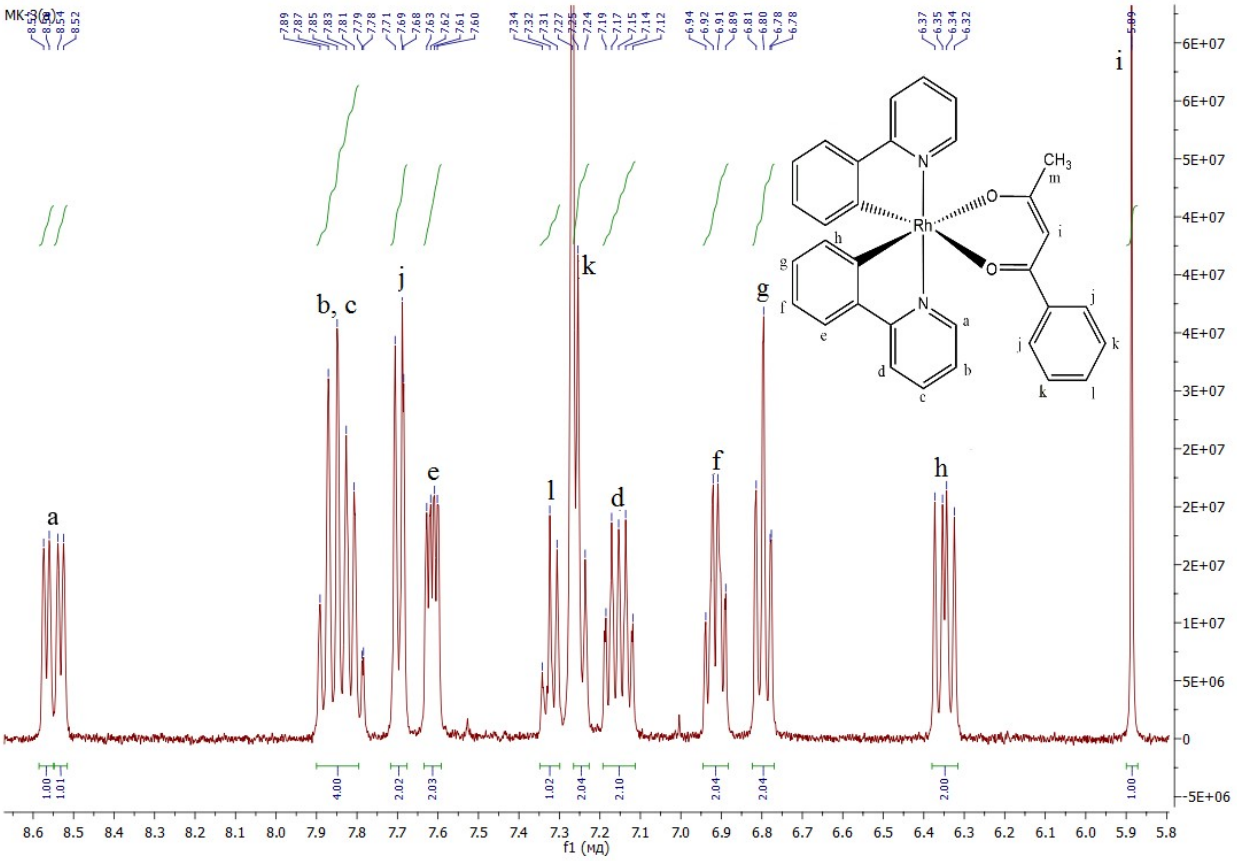

Figure S4. The aromatic part of ^{1}H NMR spectrum of **Rh2** (400 MHz, 298K, $CDCl_3$).

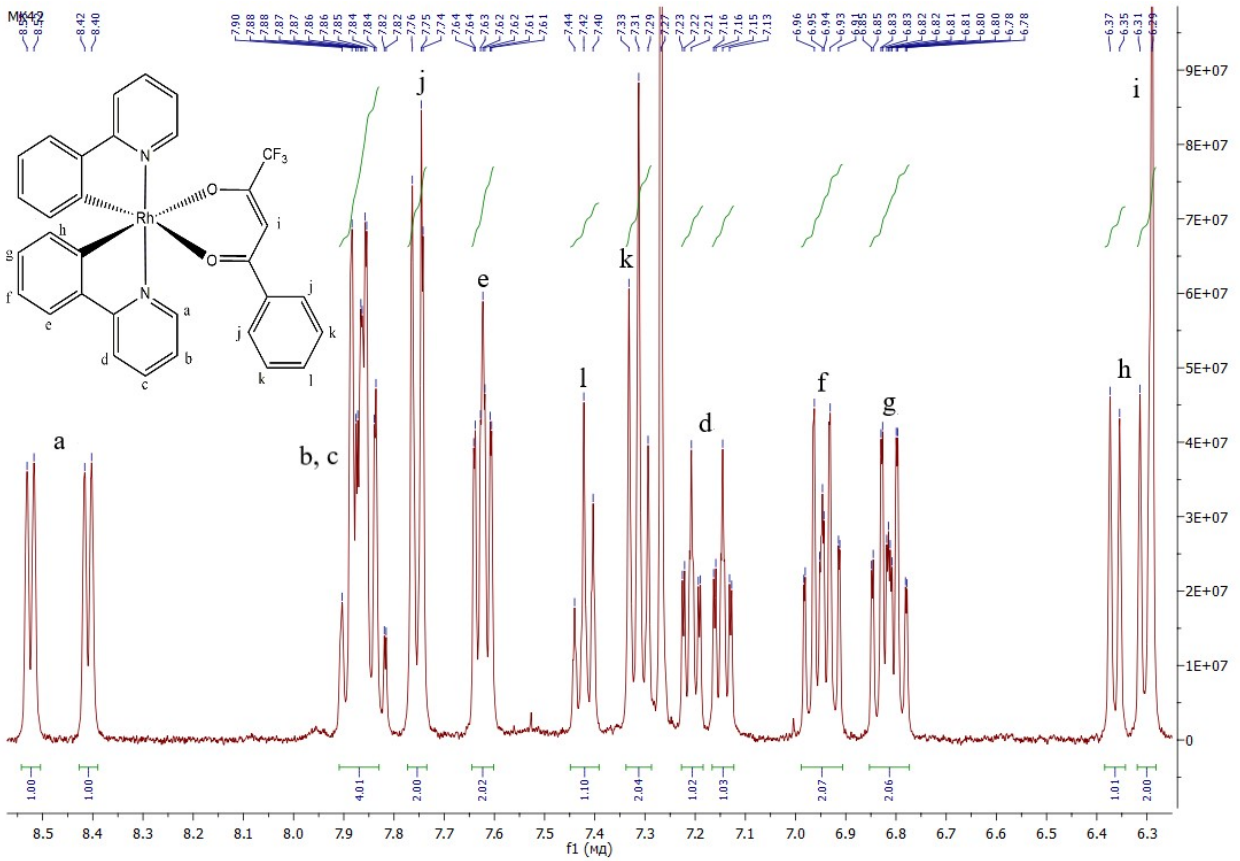

Figure S5. ^{1}H NMR spectrum of **Rh3** (400 MHz, 298K, $CDCl_3$).

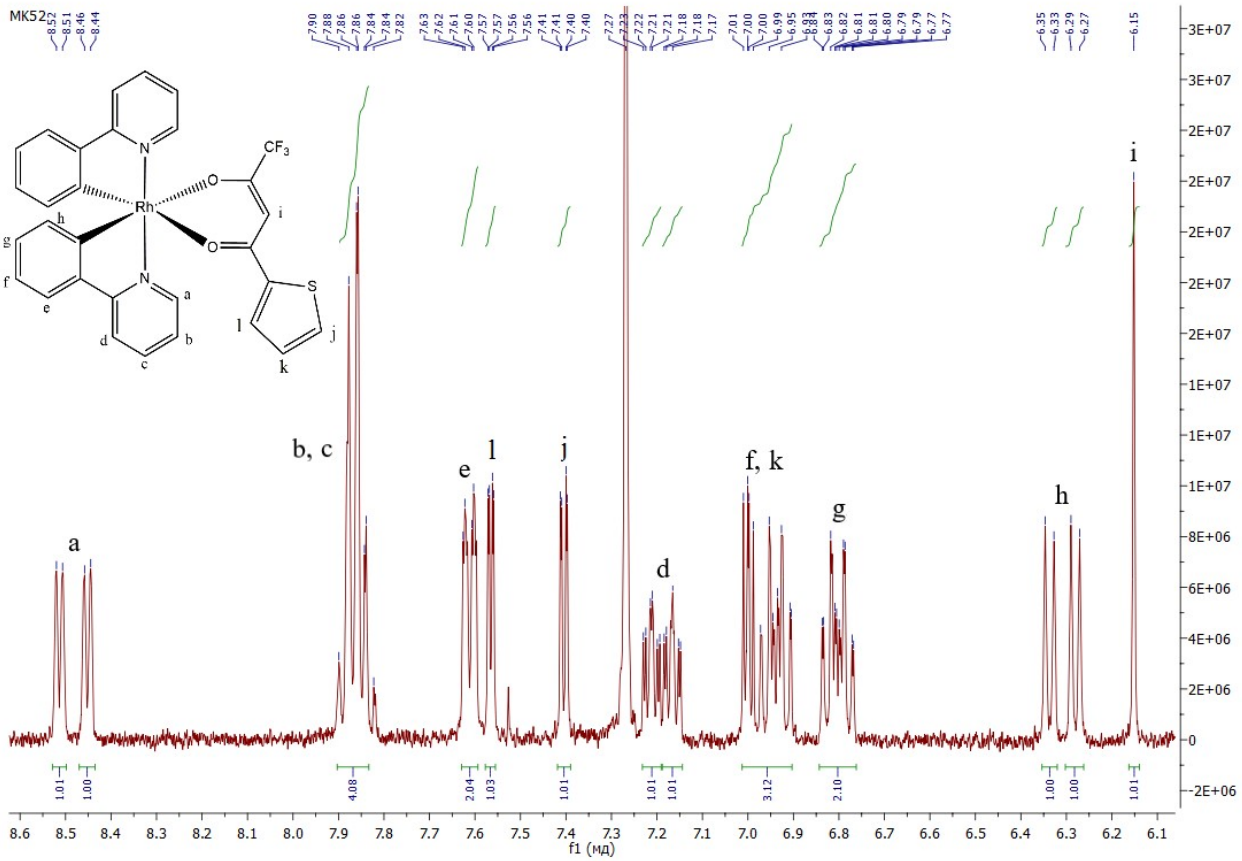

Figure S6. ^{1}H NMR spectrum of **Rh4** (400 MHz, 298K, $CDCl_3$).

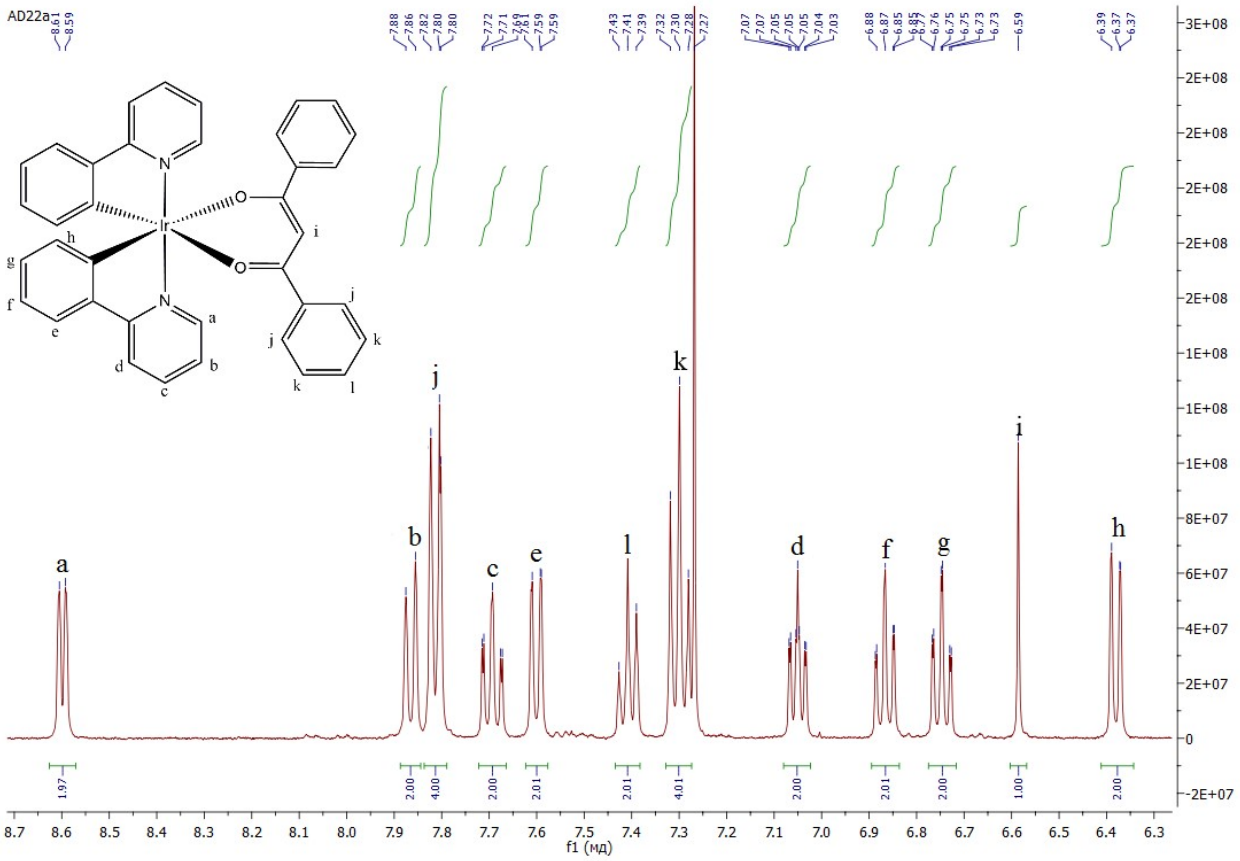

Figure S7. ^{1}H NMR spectrum of **Ir1** (400 MHz, 298K, $CDCl_3$).

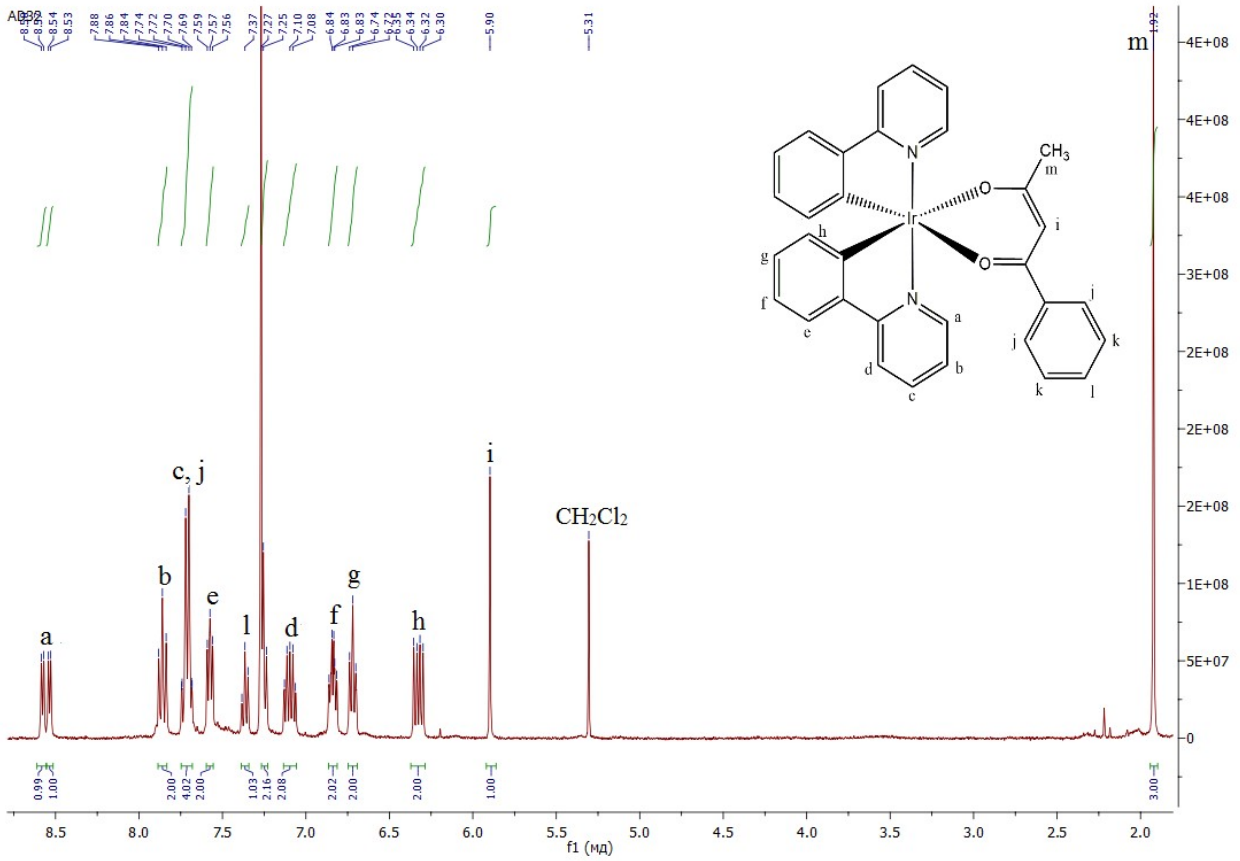

Figure S8. ^{1}H NMR spectrum of **Ir2** (400 MHz, 298K, $CDCl_3$).

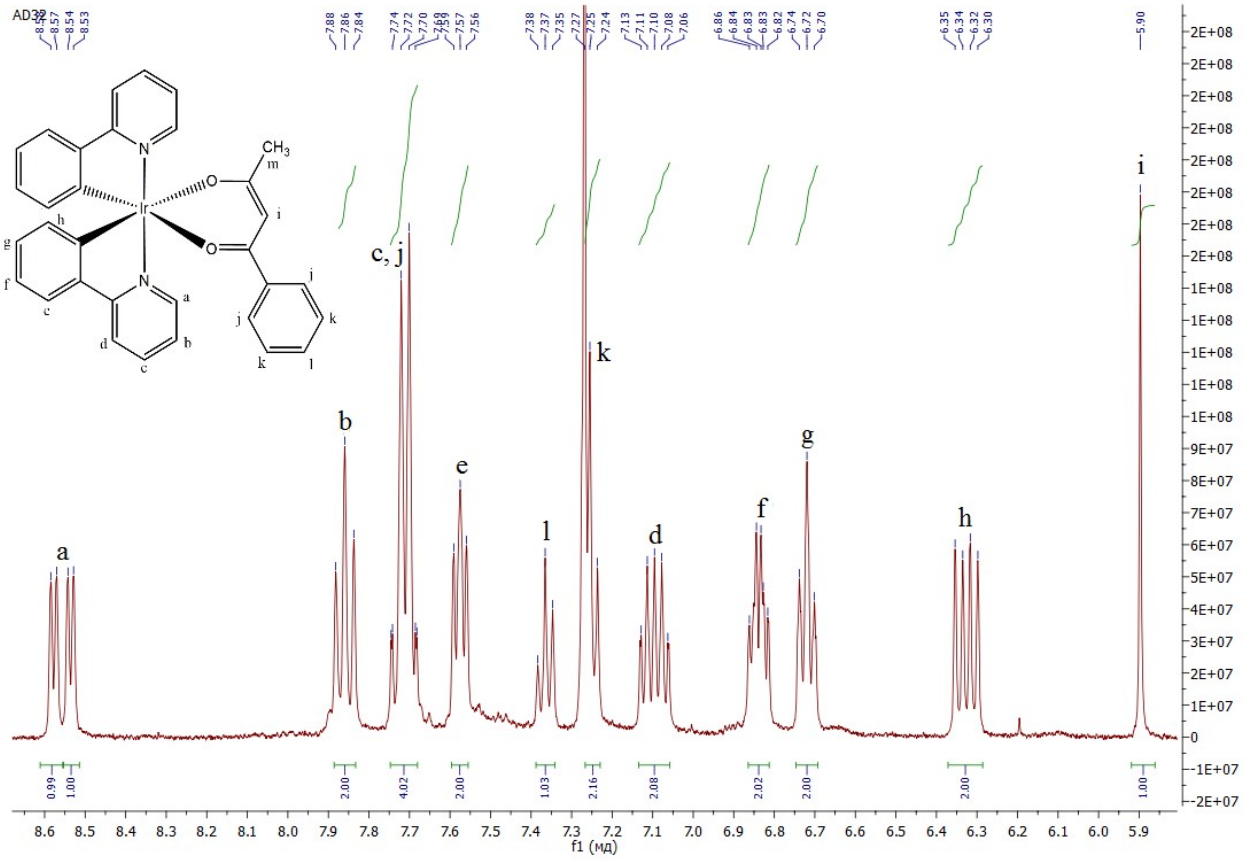

Figure S9. The aromatic part of ^{1}H NMR spectrum of **Ir2** (400 MHz, 298K, $CDCl_3$).

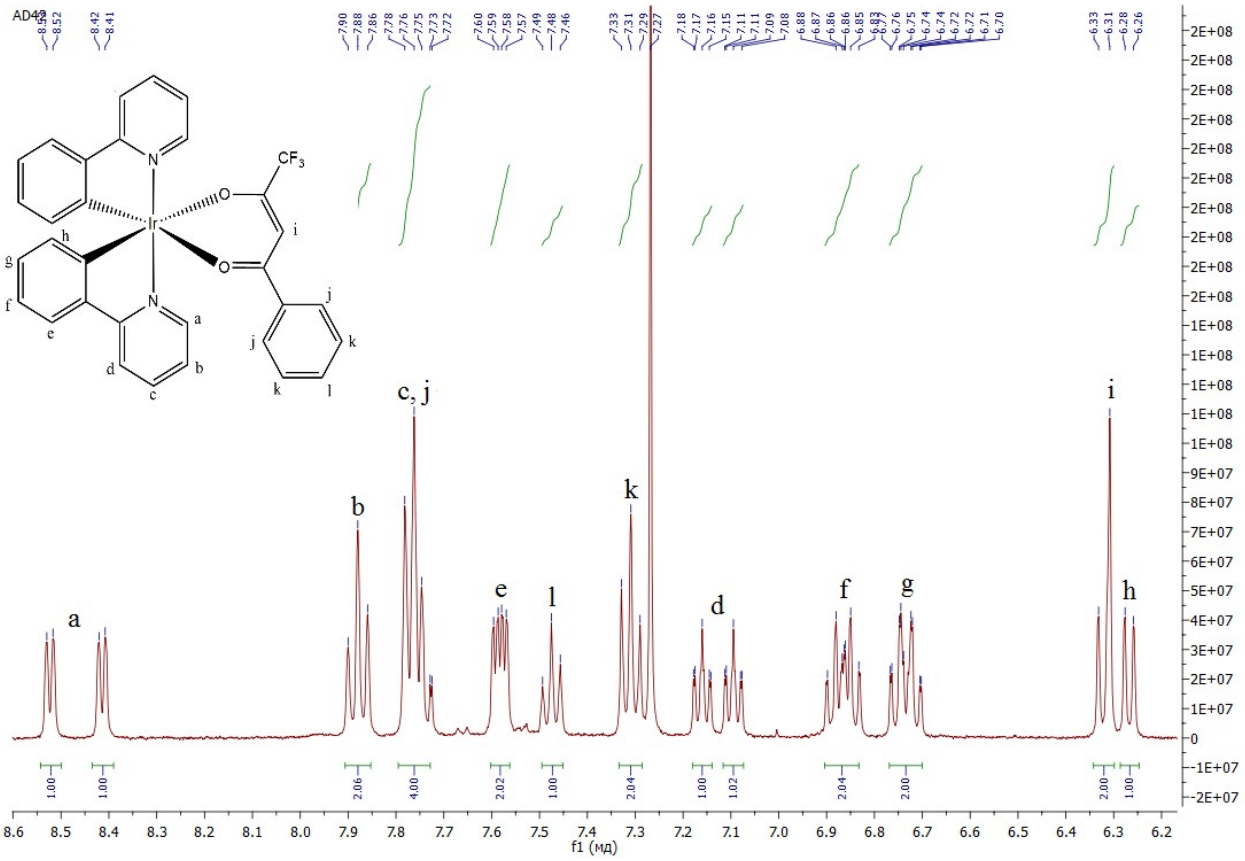

Figure S10. ^{1}H NMR spectrum of **Ir3** (400 MHz, 298K, $CDCl_3$).

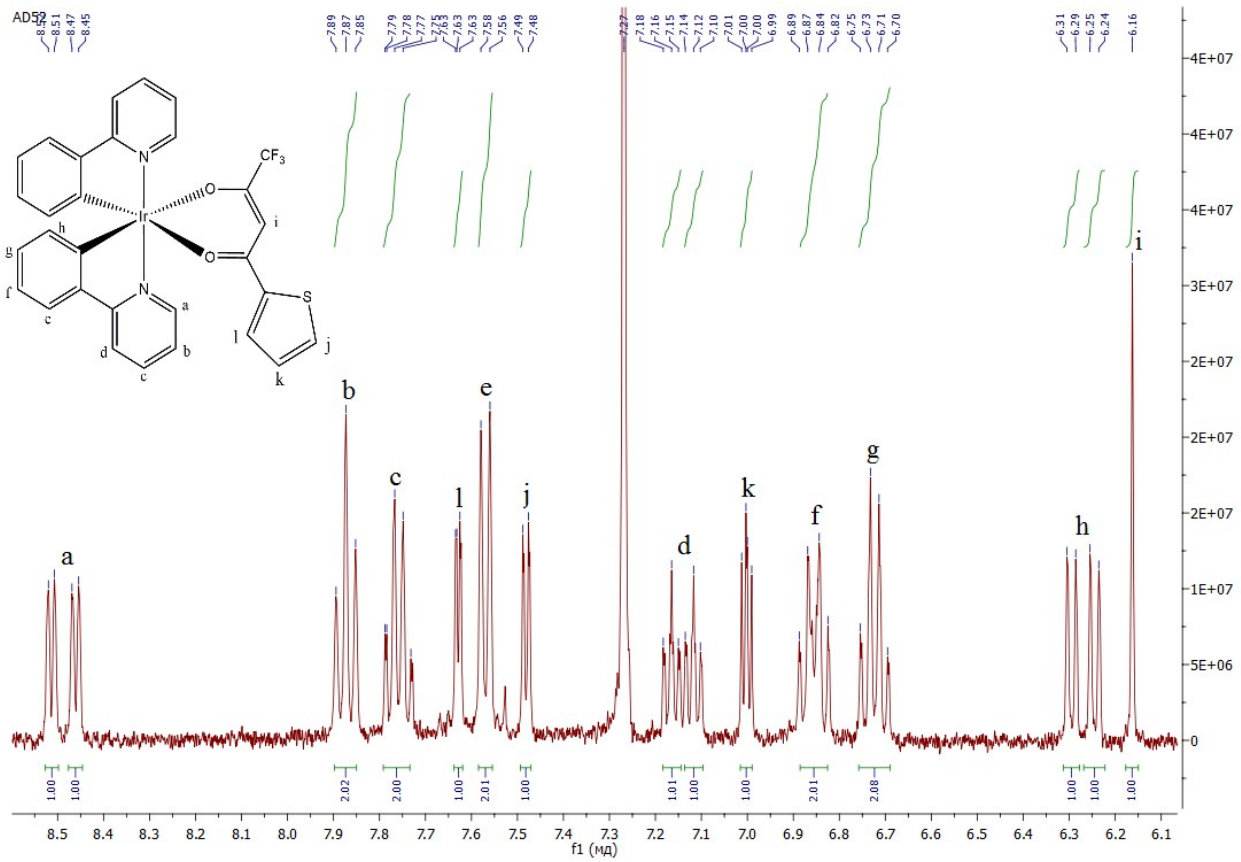

Figure S11. ^{1}H NMR spectrum of **Ir4** (400 MHz, 298K, $CDCl_3$).

Table S1. HRMS data for complexes.

Compound	$[M(ppy)_2]^+$		$[M(ppy)_2CH_3CN]^+$		$[M(ppy)_2(O^O)+H]^+$	
	Calcd	Found	Calcd	Found	Calcd	Found
Rh1	411.0369	411.0374	452.0634	452.0633	635.1201	635.1194
Rh2		411.0367		452.0627	572.0971	572.0963
Rh3		411.0364		452.0626	626.0688	626.0682
Rh4		411.0367		452.0627	632.0253	632.0243
Ir1	501.0943	501.0941	542.1208	542.1207	724.1699	724.1700
Ir2		501.0936		542.1201	662.1542	662.1540
Ir3		501.0941		542.1206	716.1259	716.1257
Ir4		501.0939		542.1206	722.0821	722.0822

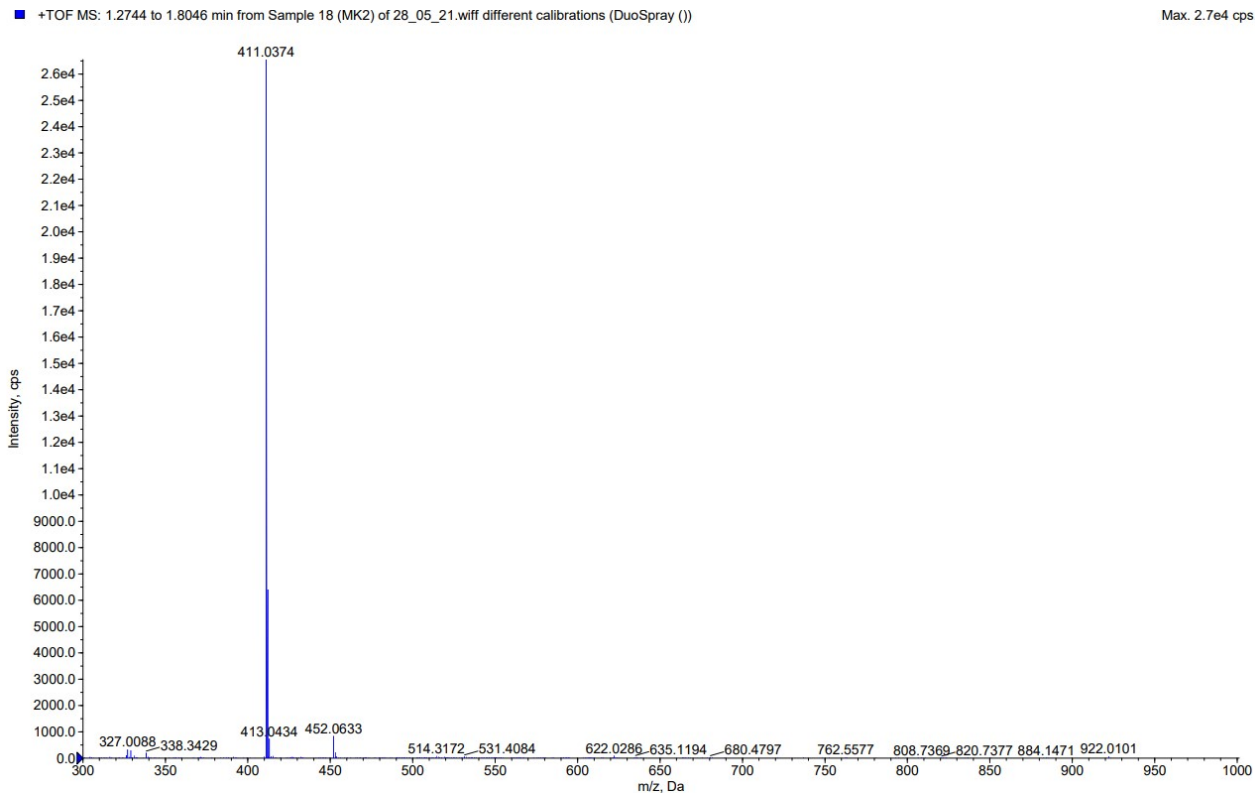

Figure S12. High-resolution mass-spectrum of **Rh1**.

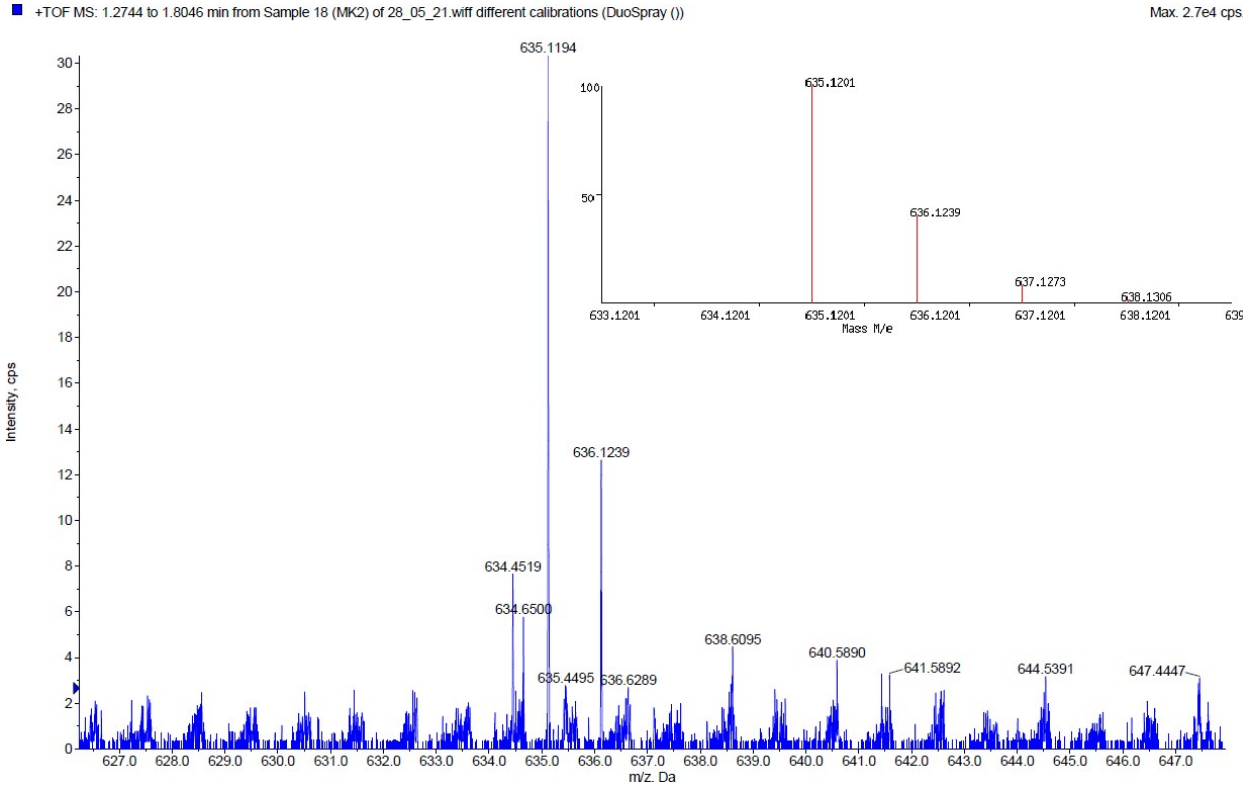

Figure S13. Fragment of high-resolution mass-spectrum of **Rh1**.

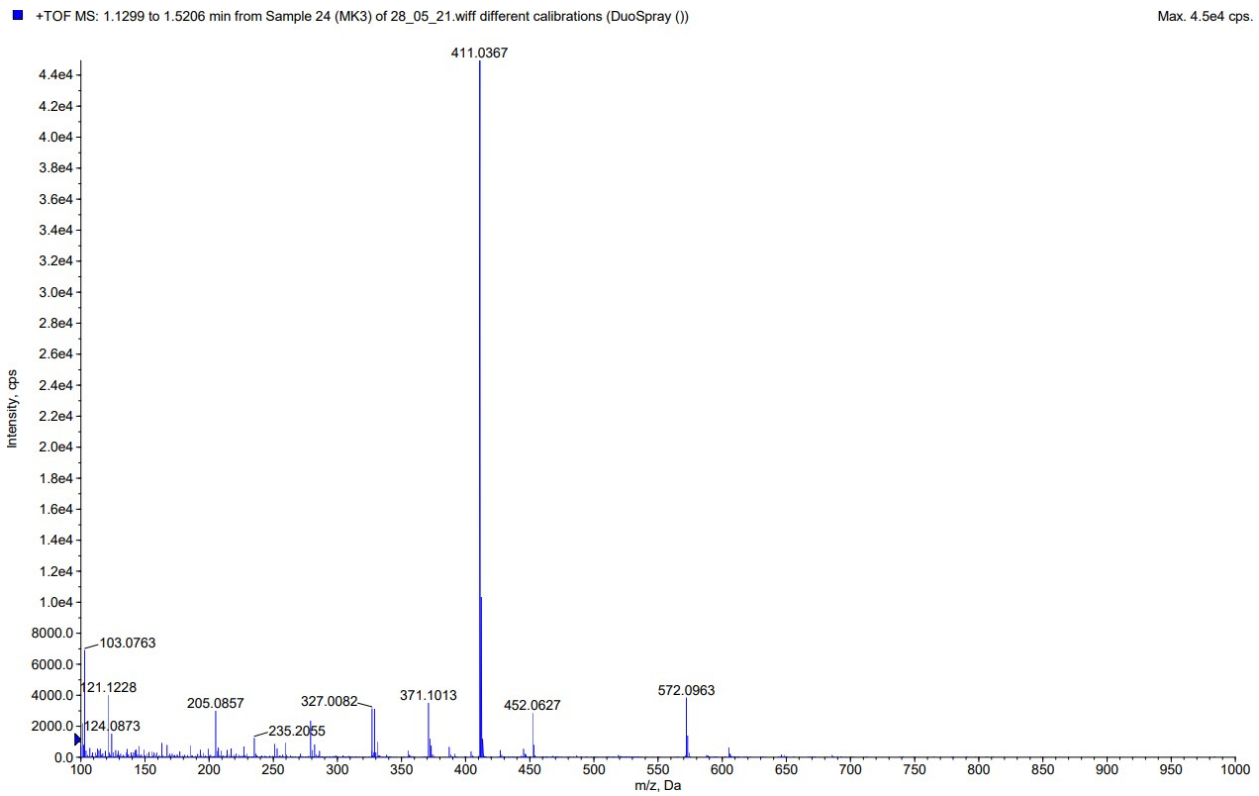

Figure S14. High-resolution mass-spectrum of **Rh2**.

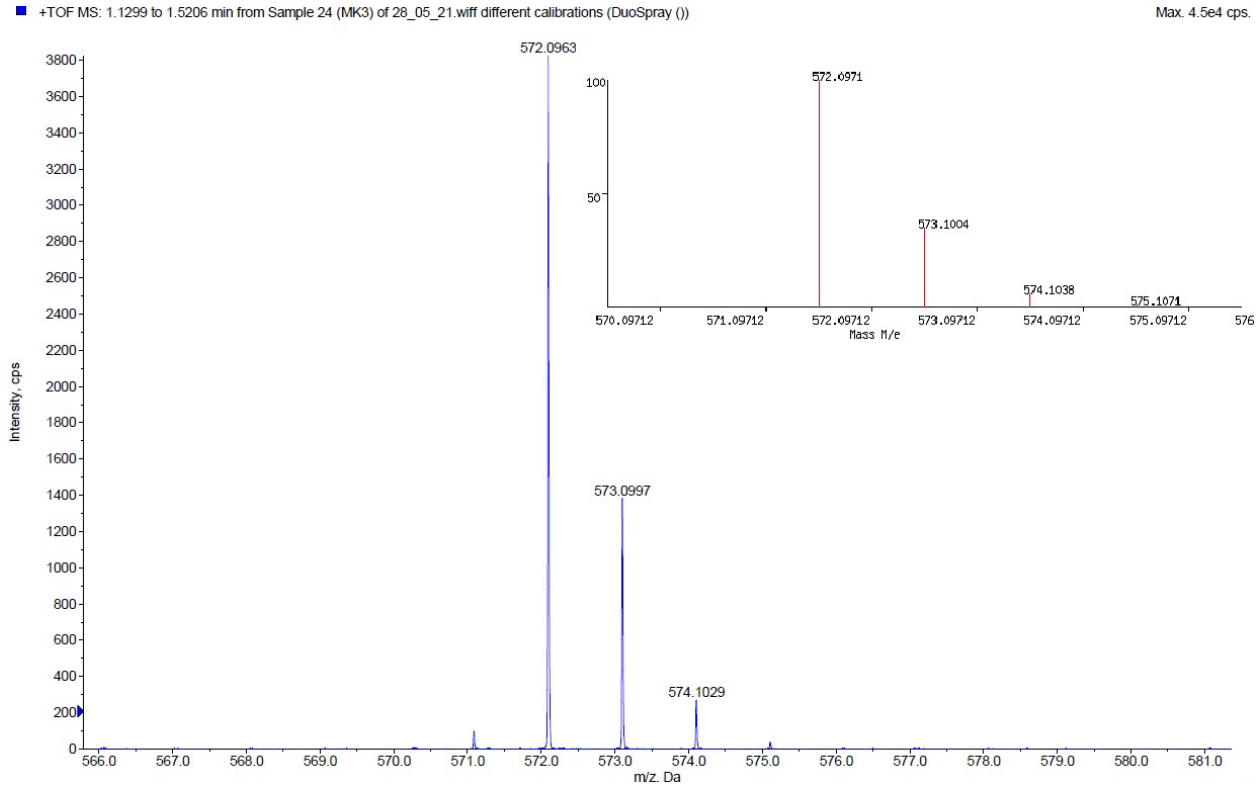

Figure S15. Fragment of high-resolution mass-spectrum of **Rh2**.

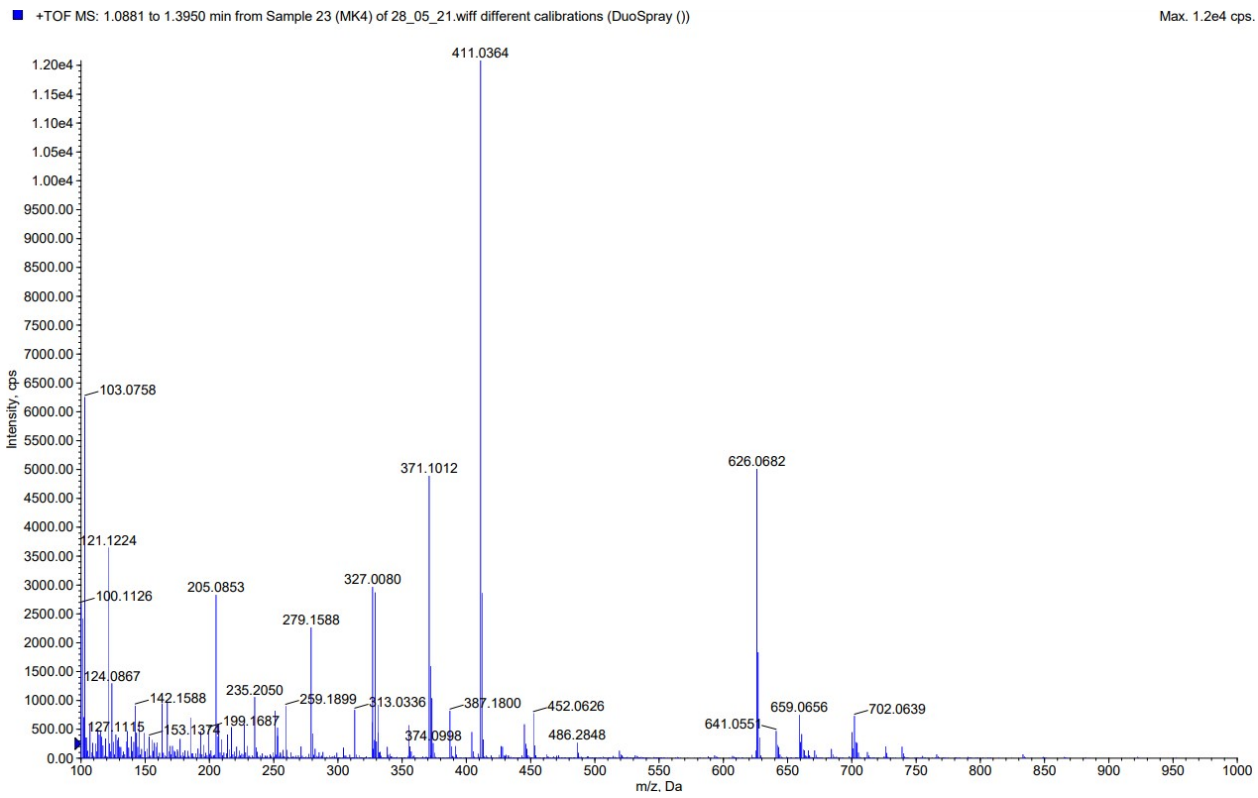

Figure S16. High-resolution mass-spectrum of **Rh3**.

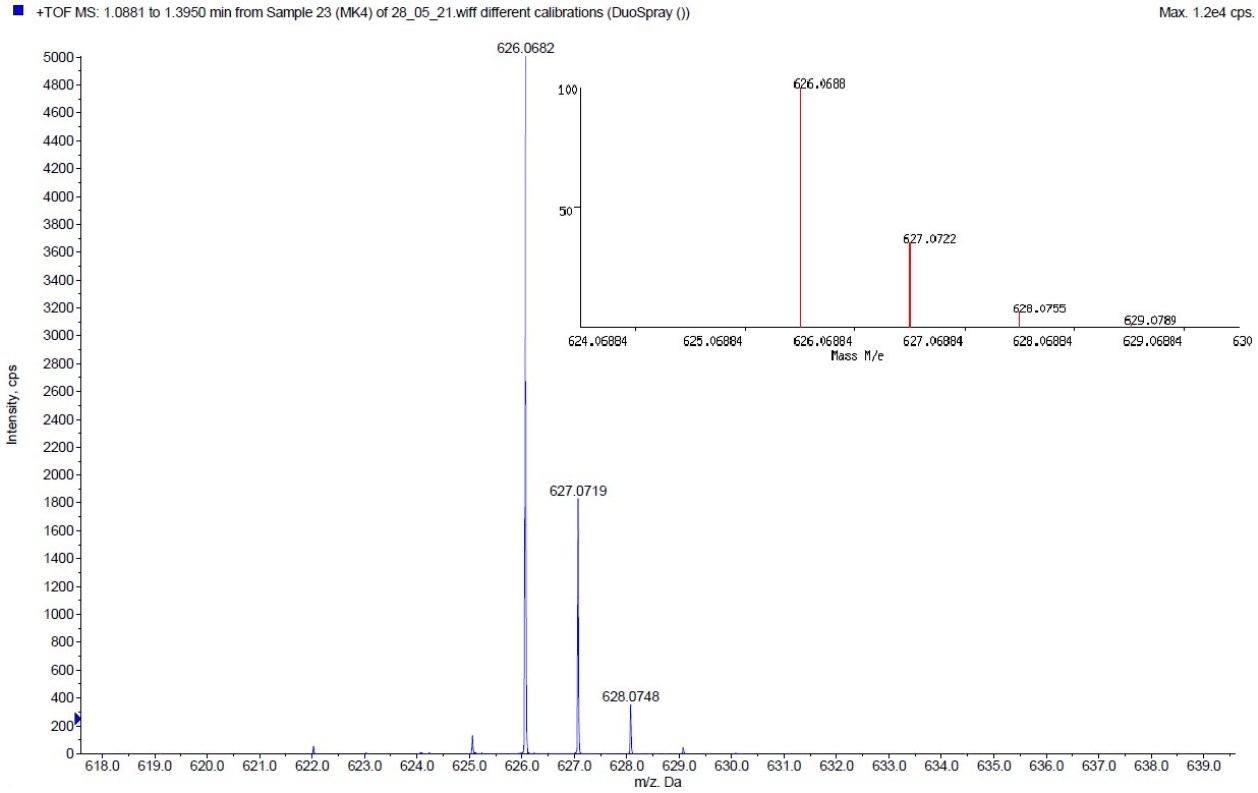

Figure S17. Fragment of high-resolution mass-spectrum of **Rh3**.

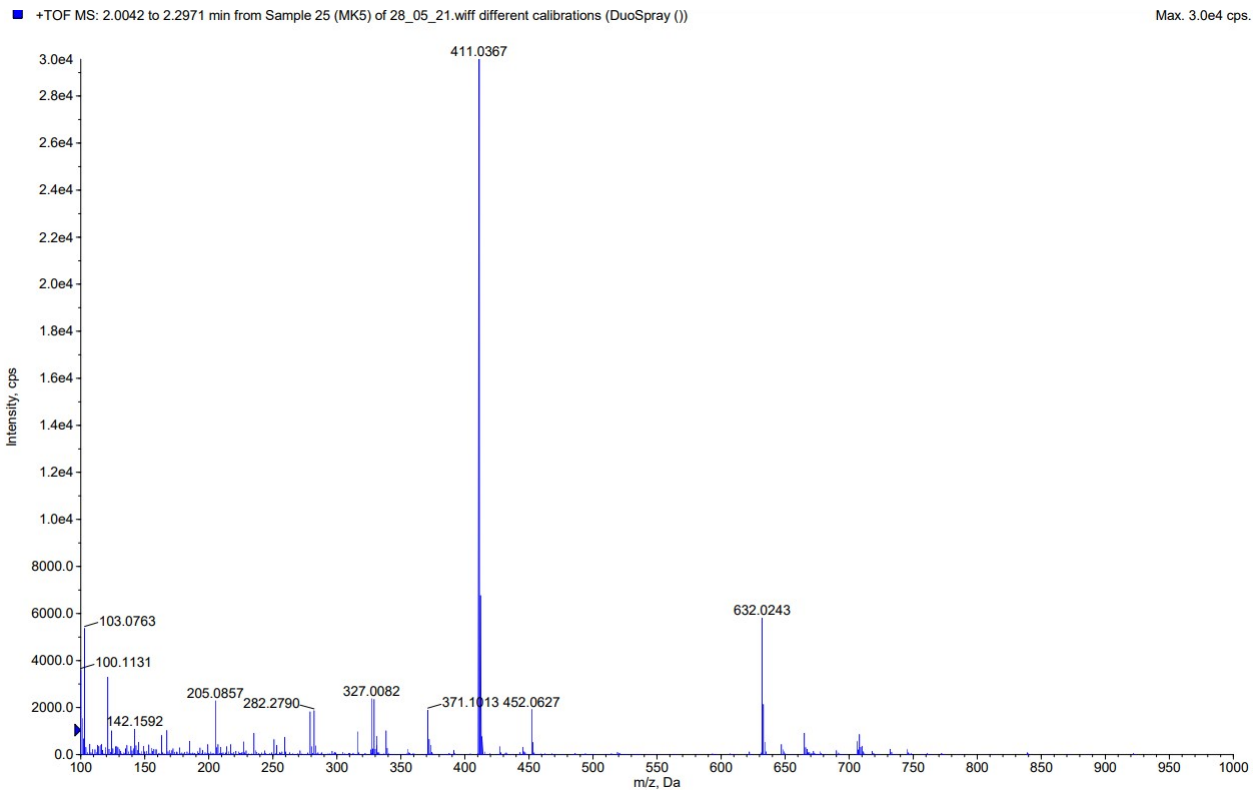

Figure S18. High-resolution mass-spectrum of **Rh4**.

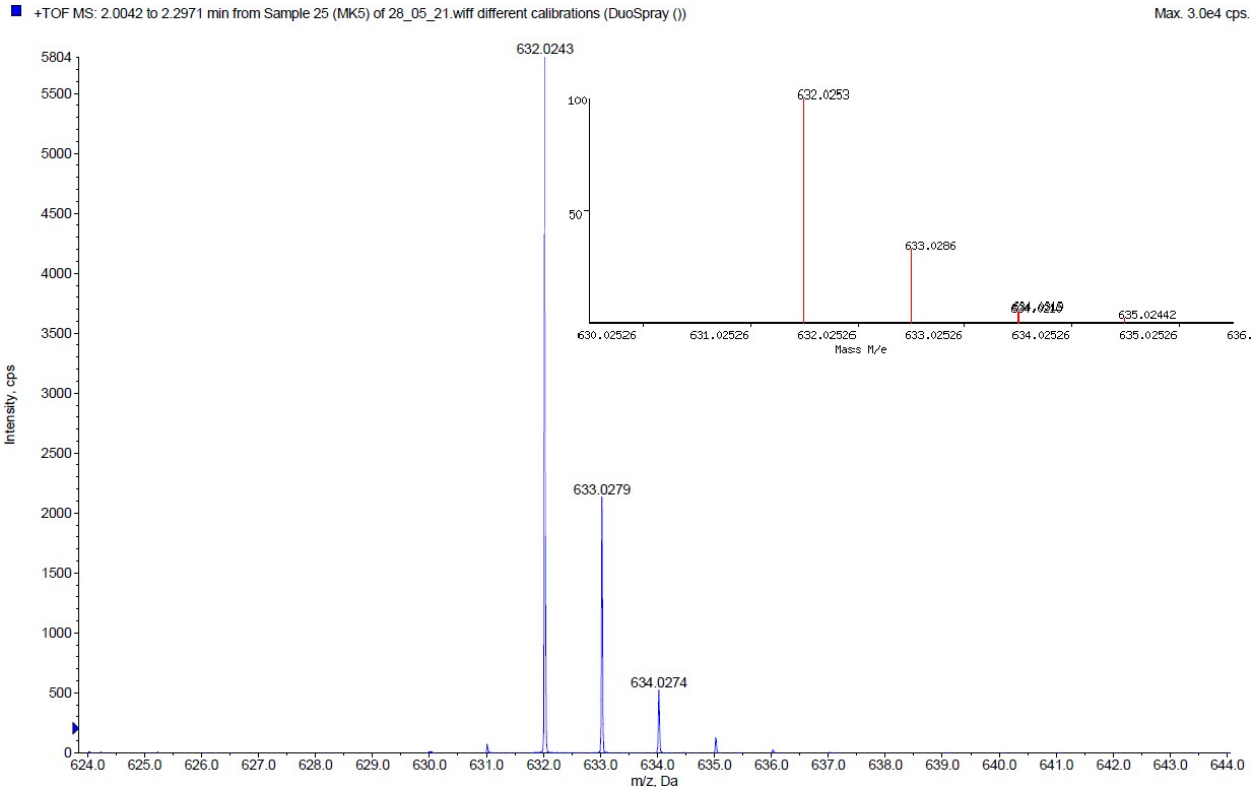

Figure S19. Fragment of high-resolution mass-spectrum of **Rh4**.

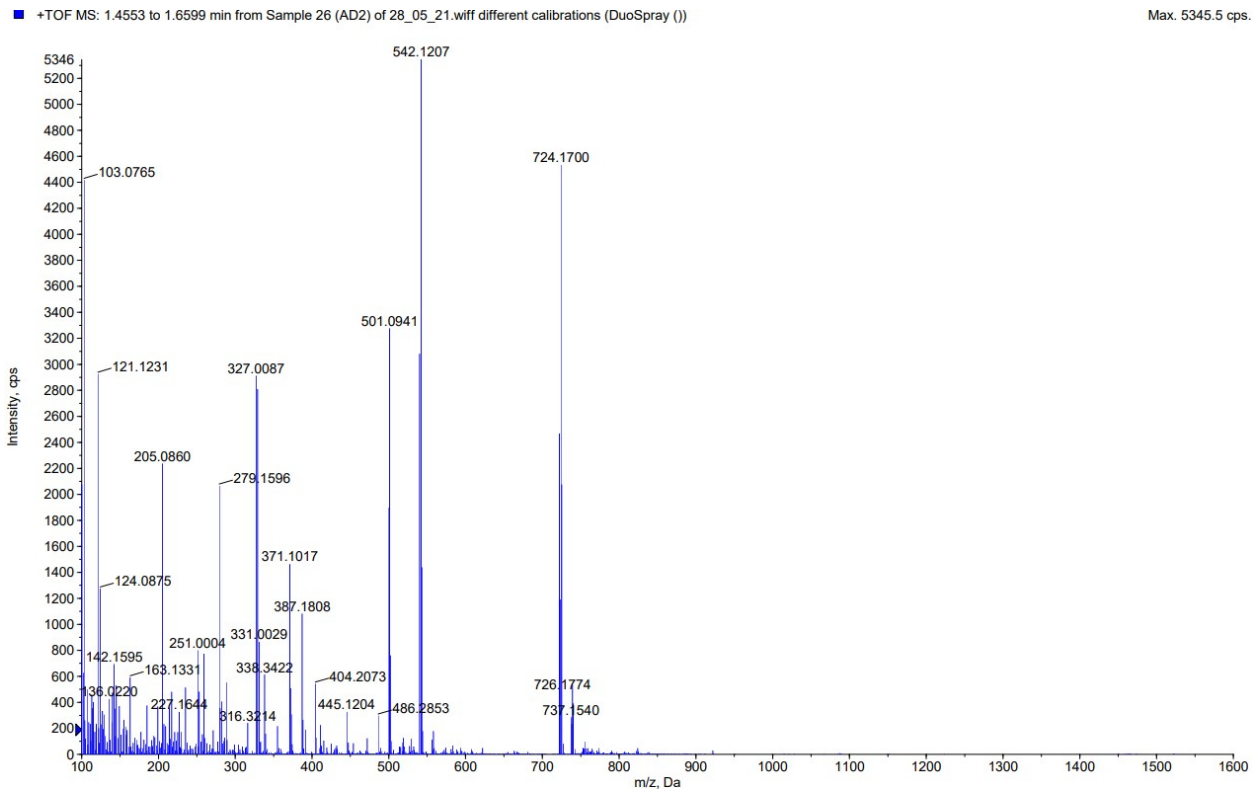

Figure S20. High-resolution mass-spectrum of **Ir1**.

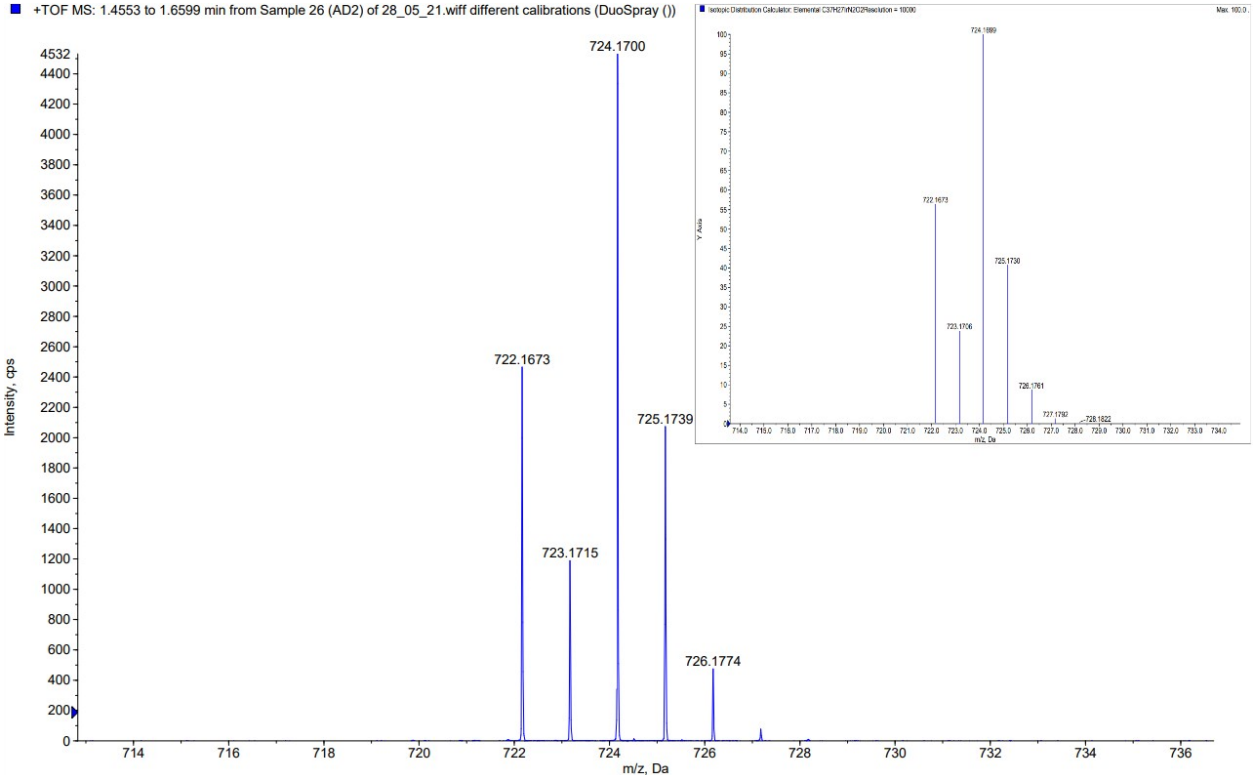

Figure S21. Fragment of high-resolution mass-spectrum of **Ir1**.

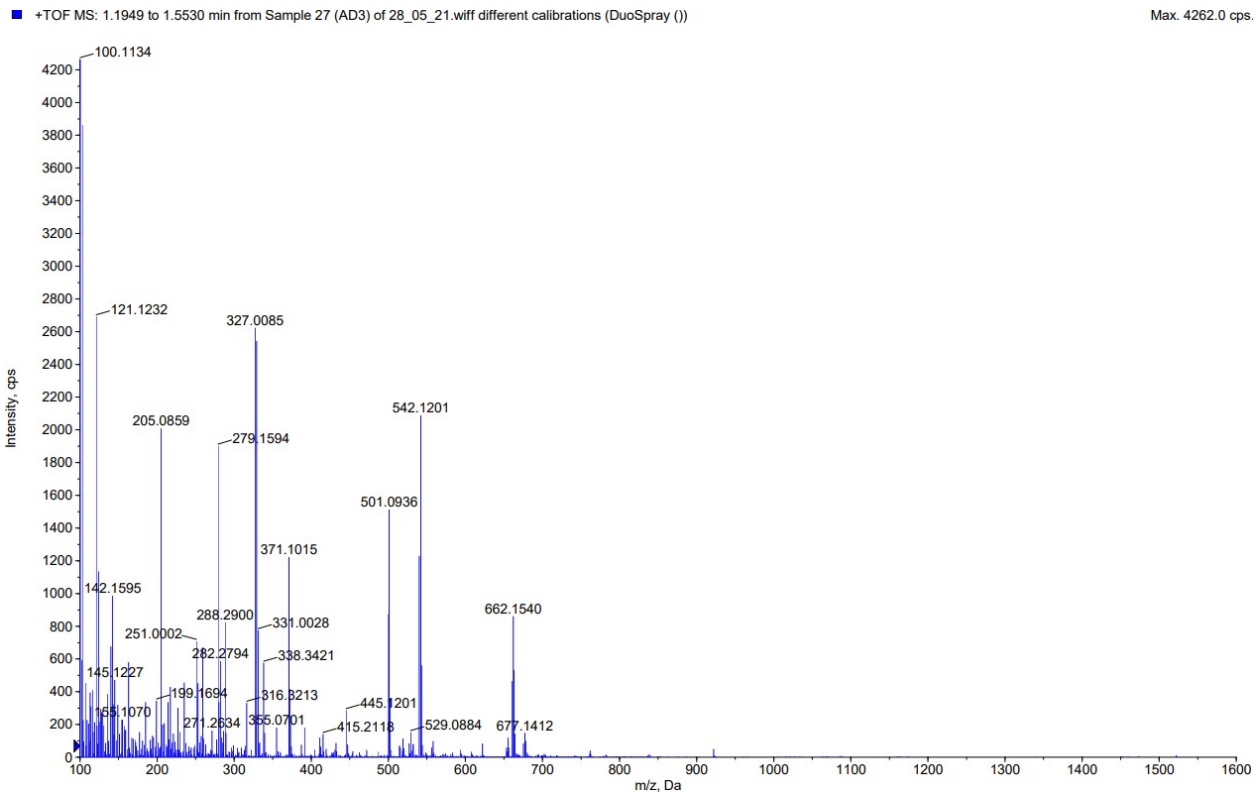

Figure S22. High-resolution mass-spectrum of **Ir2**.

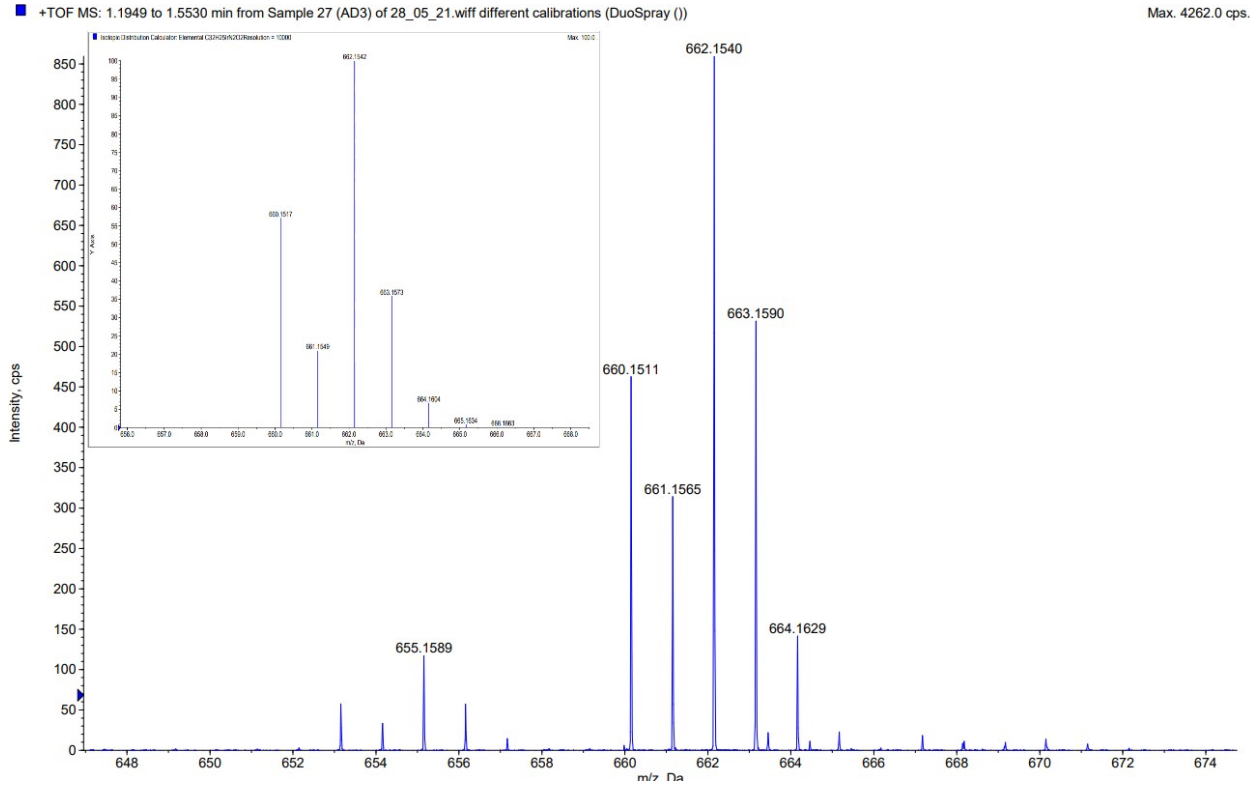

Figure S23. Fragment of high-resolution mass-spectrum of **Ir2**.

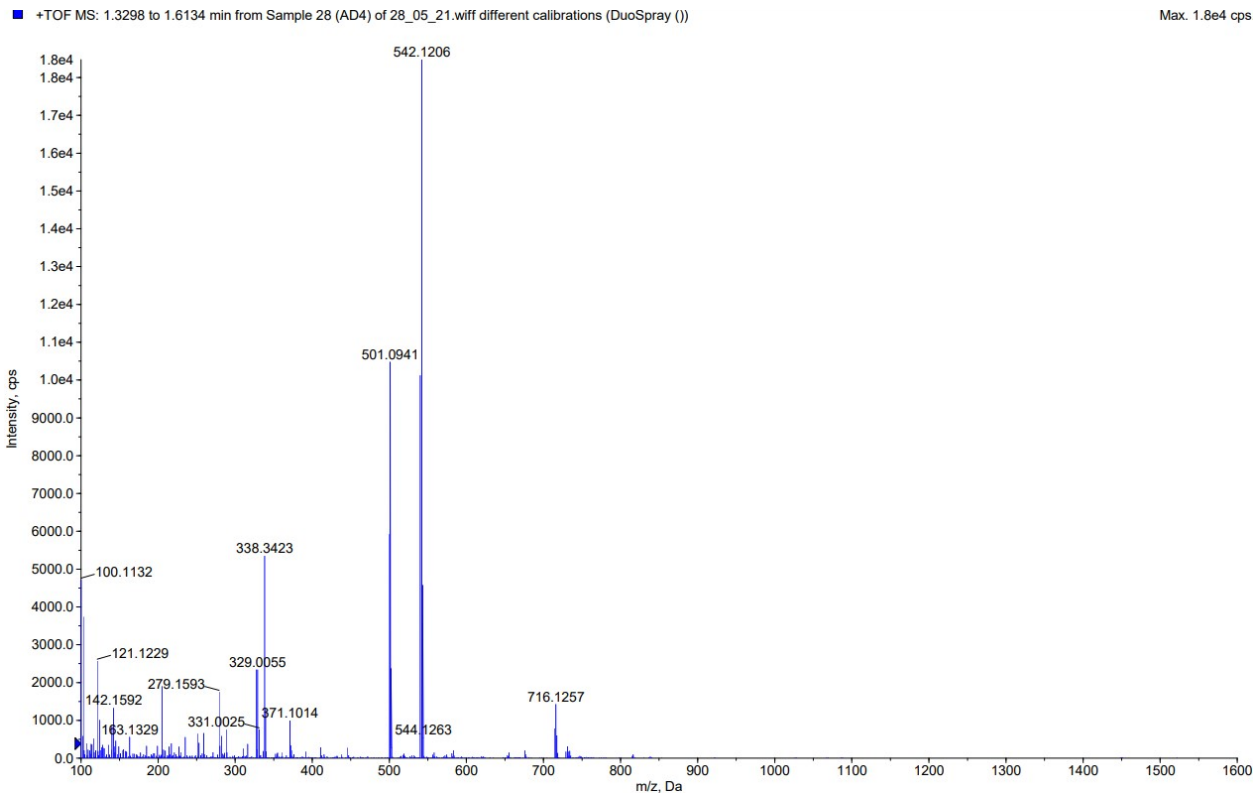

Figure S24. High-resolution mass-spectrum of **Ir3**.

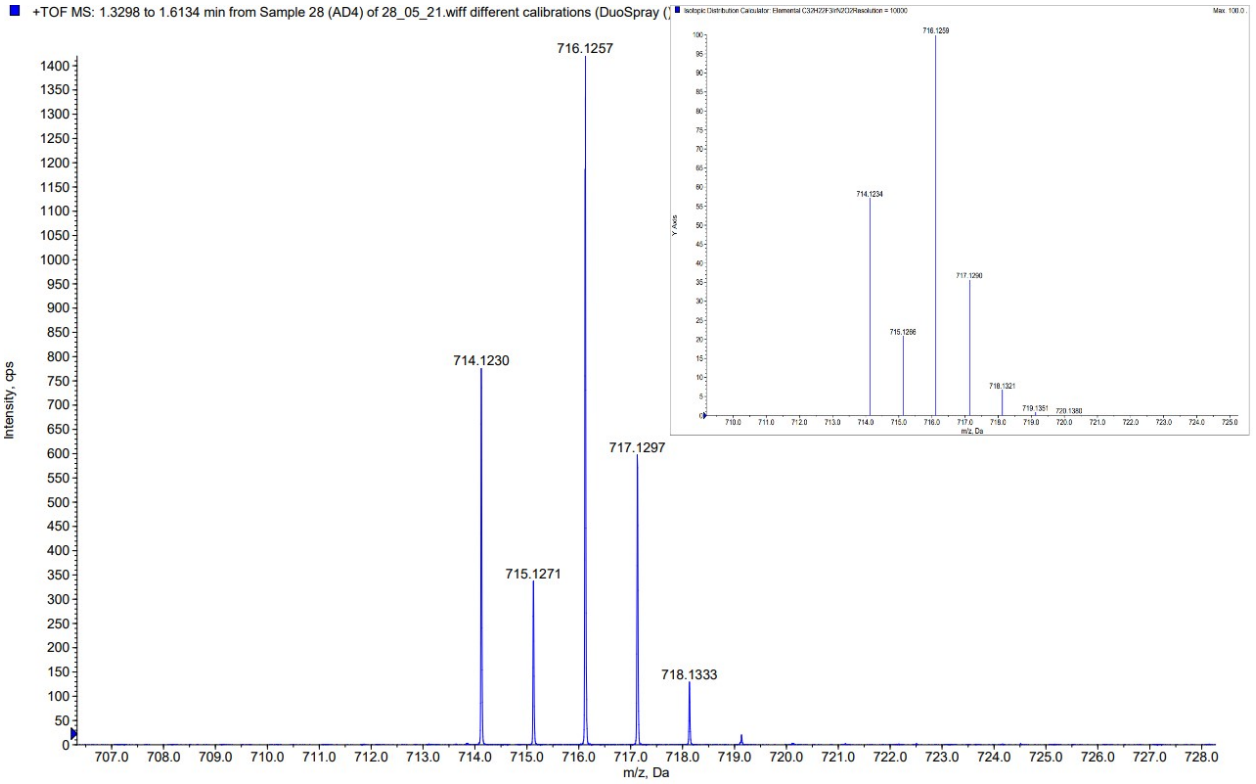

Figure S25. Fragment of high-resolution mass-spectrum of **Ir3**.

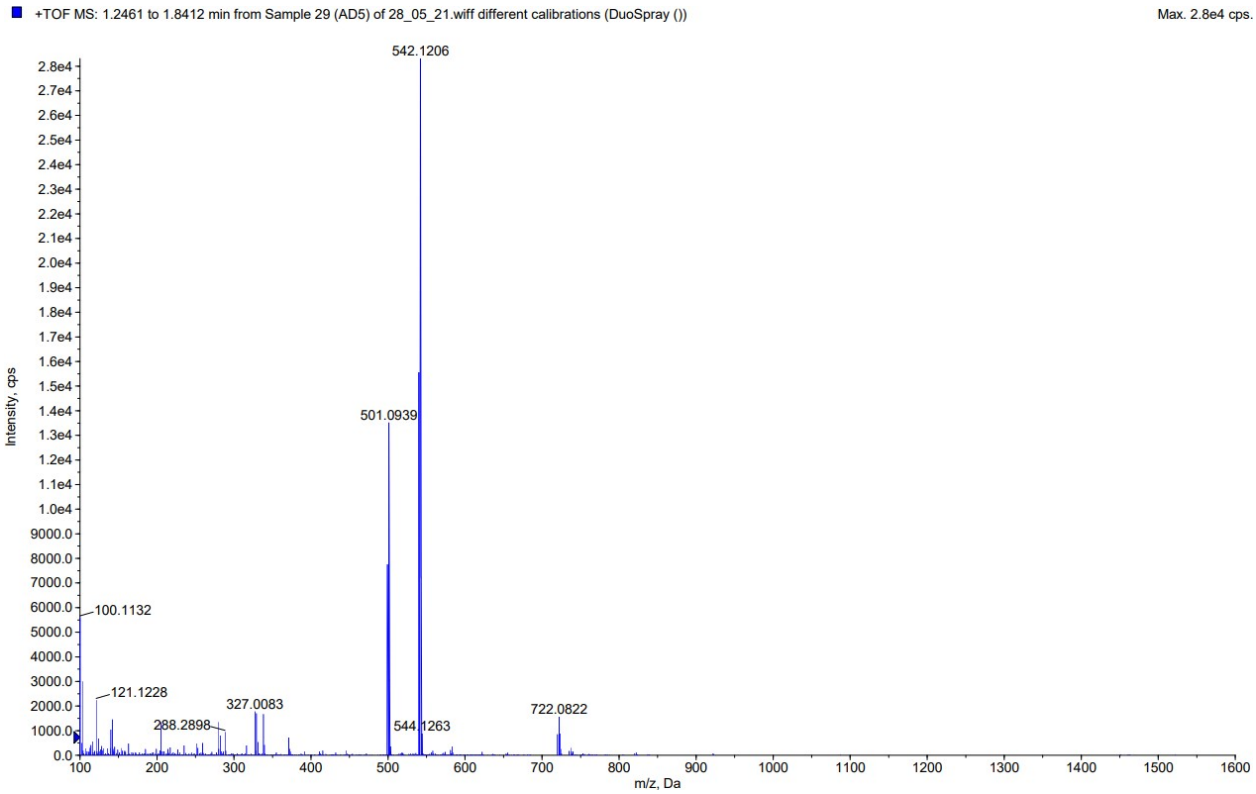

Figure S26. High-resolution mass-spectrum of **Ir4**.

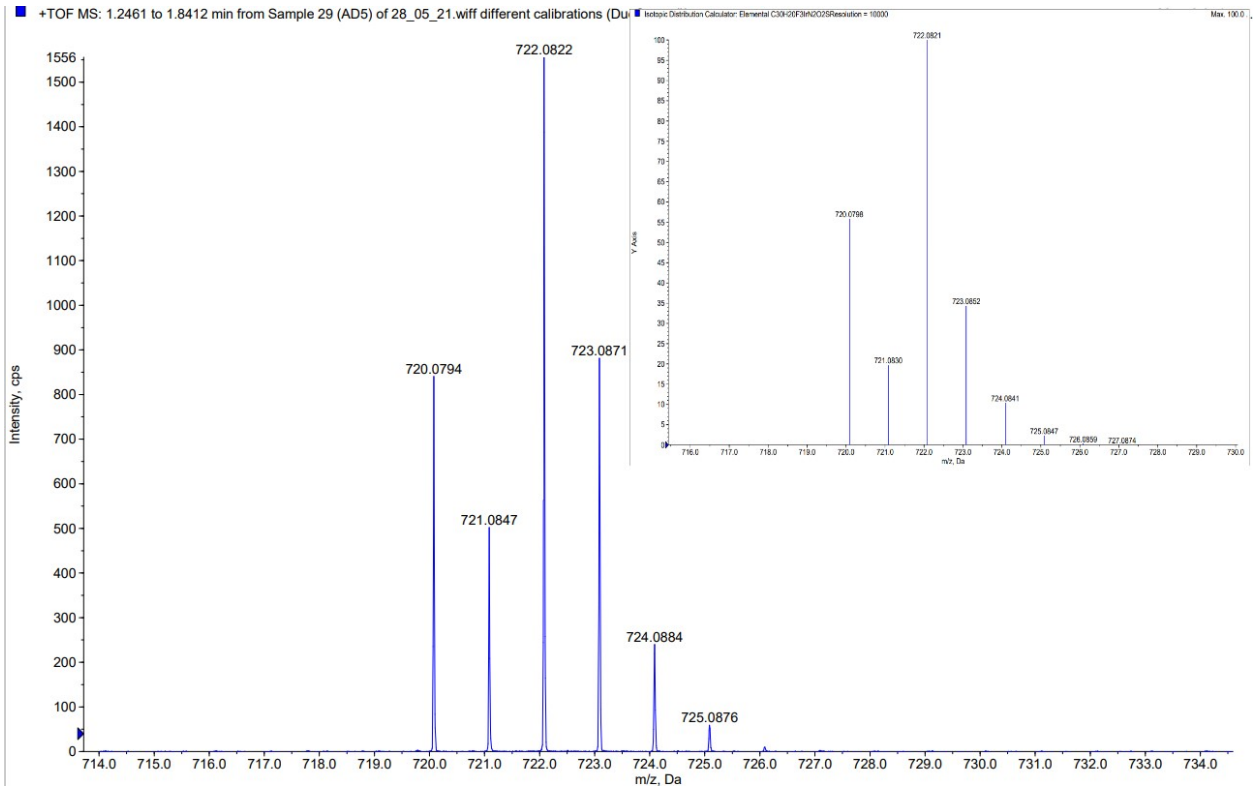

Figure S27. Fragment of high-resolution mass-spectrum of **Ir4**.

3. X-ray crystallography

Single crystals of a cyclometalated μ-chloro-bridged rhodium(III) dimer were obtained upon slow evaporation of concentrated solutions in CH_2Cl_2 or $CHCl_3$. Single crystals of **Rh1** – **Rh4** and **Ir2** – **Ir4** were obtained upon evaporation of solutions of the complexes in CH_2Cl_2/hexane (1/1 vol.). Crystallographic data were collected on Bruker SMART APEX II and D8 Venture diffractometers using graphite monochromatized Mo–Kα radiation (λ = 0.71073 Å) using a ω-scan mode. Absorption correction based on measurements of equivalent reflections was applied [4]. The structures were solved by direct methods and refined by full matrix least-squares on F^2 with anisotropic thermal parameters for all non-hydrogen atoms [5, 6]. In all structures, hydrogen atoms were placed in calculated positions and refined using a riding model. The crystal of the dimer appears as a racemic twin with the ratio of the components 0.56/0.44. In structures of b-$[Rh(ppy)_2Cl]_2$ and **Rh3, Ir2**, **Ir3**, disordered solvent molecules were not located and their contribution was suppressed by the SQUEEZE procedure [7] which is included in the Olex2 package [8]. The phenyl ring in **Rh2**, diketone in **Rh3**, thiophene rings in **Rh4**, **Ir4**, one of the C^N ligands in **Ir3** and both ppy ligands in a-$[Rh(ppy)_2Cl]_2$ are disordered over two positions with approximately equal occupancies. CCDC 2093179–2093187 contain the supplementary crystallographic data for **Ir2 – Ir4,** a-$[Rh(ppy)_2Cl]_2$, b-$[Rh(ppy)_2Cl]_2$, **Rh1 – Rh4**, respectively. These data can be obtained free of charge from The Cambridge Crystallographic Data Centre via www.ccdc.cam.ac.uk/data_request/cif.

Table S2. Details of the X-ray crystal data collection and structure refinement for complexes **Rh1 – Rh4, Ir2 – Ir4, $[Rh(ppy)_2Cl]_2$.**

	Rh1	**Rh2**	**Rh3**	**Rh4**	**Ir2**	**Ir3**	**Ir4**	**a-$[Rh(ppy)_2Cl]_2$**	**b-$[Rh(ppy)_2Cl]_2$**
Empirical formula	$C_{37.5}H_{28}ClN_2O_2Rh$	$C_{32}H_{25}N_2O_2Rh$	$C_{32}H_{22}F_3N_2O_2Rh$	$C_{30}H_{20}F_3N_2O_2RhS$	$C_{32}H_{25}IrN_2O_2$	$C_{32}H_{22}F_3IrN_2O_2$	$C_{30}H_{20}F_3IrN_2O_2S$	$C_{44}H_{32}Cl_2N_4Rh_2$	$C_{44}H_{32}Cl_2N_4Rh_2$
M_w	676.98	572.45	626.42	632.45	661.74	715.71	721.74	893.45	893.45
Temperature (K)	100	100	150	150	100	150	100	100.15	100
Size (mm)	0.32x0.18x0.04	0.13x0.08x0.01	0.18x0.05x0.03	0.21x0.15x0.05	0.16x0.12x0.09	0.23x0.15x0.12	0.22x0.14x0.11	0.12x0.1x0.01	0.22x0.2x0.08
Cryst. system	triclinic	monoclinic	triclinic	monoclinic	monoclinic	triclinic	monoclinic	monoclinic	monoclinic
Space group	P–1	$P2_1/n$	P–1	$P2_1/c$	$P2_1/n$	P–1	$P2_1/c$	Pc	$P2_1/n$
a (Å)	10.5699(2)	10.0427(11)	11.4135(4)	15.4022(5)	10.1004(5)	11.4446(6)	15.3589(12)	12.7993(8)	13.4265(12)
b (Å)	11.7403(2)	23.901(2)	11.8344(4)	20.3286(6)	23.8644(13)	11.7077(6)	20.2331(16)	17.6551(10)	13.9065(11)
c (Å)	12.2502(2)	12.1579(12)	13.4479(5)	17.4956(6)	12.1714(6)	13.0847(7)	17.6076(15)	16.4434(10)	24.1630(18)
α(°)	92.2610(10)	90	70.7650(10)	90	90	71.158(2)	90	90	90
β (°)	93.1600(10)	100.002(4)	72.2520(10)	112.9990(10)	100.722(2)	75.027(2)	113.797(2)	108.775(2)	95.936(3)
γ(°)	104.3880(10)	90	67.1520(10)	90	90	67.214(2)	90	90	90
V (Å^3)	1468.03(4)	2874.0(5)	1547.45(10)	5042.5(3)	2882.6(3)	1511.82(14)	5006.5(7)	3518.0(4)	4487.4(6)
Z	2	4	2	8	4	2	8	4	4
ρ_{cald} (g·cm^{-3})	1.532	1.323	1.344	1.666	1.525	1.572	1.915	1.687	1.322
Abs coeff (mm^{-1})	0.711	0.623	0.598	0.815	4.661	4.464	5.473	1.130	0.886
F(000)	690.0	1168.0	632.0	2544.0	1296.0	696.0	2800.0	1792.0	1792.0
θ range (deg)	2.32< *θ* < 30.52	2.41<*θ*<22.49	2.24< *θ* < 28.83	2.37 < *θ* < 28.29	2.41<*θ*<25.25	1.95<*θ*<26.00	2.35< *θ* <26.12	2.615<*θ*<30.549	2.22<*θ*<28.28
collected/unique rflns	18790 / 8818	29915 / 5057	38065 / 9430	58653 / 12448	41193 / 5104	17126 / 5881	71238 / 10933	29400 / 14878	44352 / 9749
Completeness to *θ* (%)	98.2	99.9	99.6	99.3	97.7	99.0	100.0	96.9	99.6
no. of data/restraints/params	8818 / 1 / 397	5057 / 0 / 305	9430 / 18 / 328	12448 / 22 / 691	5104 / 0 / 335	5881 / 2 / 307	10933 / 8 / 697	14878 / 2 / 914	9749 / 2 / 409
Goodness of fit on F^2	1.040	1.028	1.035	1.019	1.040	1.054	1.007	1.373	1.026
Final *R* indices ($I > 2\sigma(I)$)	R_1 = 0.0307, wR_2 = 0.0718	R_1 = 0.0600, wR_2 = 0.1338	R_1 = 0.0492, wR_2 = 0.1221	R_1 = 0.0378, wR_2 = 0.0807	R_1 = 0.0363, wR_2 = 0.0815	R_1 = 0.0342, wR_2 = 0.0821	R_1 = 0.0360, wR_2 = 0.0655	R_1 = 0.0765, wR_2 = 0.2100	R_1 = 0.0552, wR_2 = 0.1394
R indices (all data)	R_1 = 0.0342, wR_2 = 0.0736	R_1 = 0.0964, wR_2 = 0.1478	R_1 = 0.0588, wR_2 = 0.1276	R_1 = 0.0515, wR_2 = 0.0861	R_1 = 0.0521, wR_2 = 0.0875	R_1 = 0.0386, wR_2 = 0.0839	R_1 = 0.0669, wR_2 = 0.0753	R_1 = 0.0986, wR_2 = 0.2214	R_1 = 0.0746, wR_2 = 0.1503
Largest diff peak/hole (e/Å^3)	1.58/–1.71	0.74/–0.84	2.62/–0.97	1.53/–1.32	1.13/–1.57	2.89/–1.03	1.65/–1.41	1.77/–2.22	1.18/–1.63

Table S3. Unit cell parameters for **Rh1** – **Ir4** based on single-crystal and powder X-ray data.

Complex		a, Å	b, Å	c, Å	α, °	β, °	γ, °	V, Å^3
Rh1	Powder	10.6568(14)	11.7494(10)	12.2811(15)	91.950(17)	93.376(12)	104.516(12)	1484.2(4)
	Single-crystal	10.5699(2)	11.7403(2)	12.2502(2)	92.2610(10)	93.1600(10)	104.3880(10)	1468.03(4)
Rh2	Powder	9.6386(15)	23.717(2)	12.1228(15)	90	100.082(11)	90	2728.7(5)
	Single-crystal	10.0427(11)	23.901(2)	12.1579(12)	90	100.002(4)	90	2873.9(5)
Rh3	Powder	10.1895(18)	12.9099(17)	13.1533(19)	70.741(10)	73.636(11)	68.389(10)	1493.1(7)
	Single-crystal	11.4135(4)	11.8344(4)	13.4479(5)	70.7650(10)	72.2520(10)	67.1520(10)	1547.45(10)
Rh4	Powder	14.8575(19)	20.3343(17)	17.9261(12)	90	112.242(6)	90	5012.6(3)
	Single-crystal	15.4022(5)	20.3286(6)	17.4956(6)	90	112.9990(10)	90	5042.5(3)
Ir1	Powder	10.9515(15)	11.2465(12)	12.4657(19)	94.258(12)	91.934(14)	103.479(9)	1484.3(6)
	Single-crystal	10.8400(7)	11.6907(8)	12.3687(9)	94.632(2)	92.666(2)	102.807(2)	1520.11(18)
Ir2	Powder	10.305(3)	24.832(5)	12.097(3)	90	103.642(16)	90	3000.4(12)
	Single-crystal	10.1004(5)	23.8644(13)	12.1714(6)	90	100.722(2)	90	2882.6(3)
Ir3	Powder	11.195(3)	12.413(3)	13.387(3)	69.299(16)	75.706(16)	67.340(12)	1592.5(13)
	Single-crystal	11.4446(6)	11.7077(6)	13.0847(7)	71.158(2)	75.027(2)	67.214(2)	1511.82(14)
Ir4	Powder	15.4621(11)	20.1555(14)	17.8598(14)	90	113.436(7)	90	5102.9(7)
	Single-crystal	15.3589(12)	20.2331(16)	17.6076(15)	90	113.797(2)	90	5006.5(7)

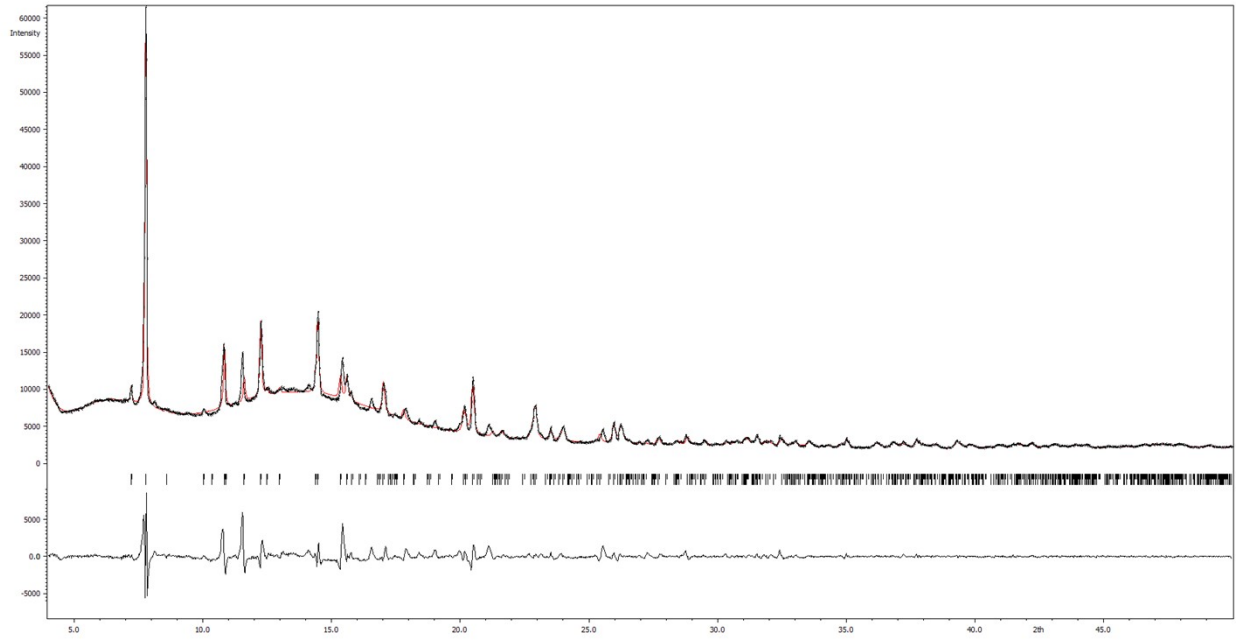

Figure S28. Experimental (black) and simulated (red) X-ray powder diffraction patterns of **Rh1**.

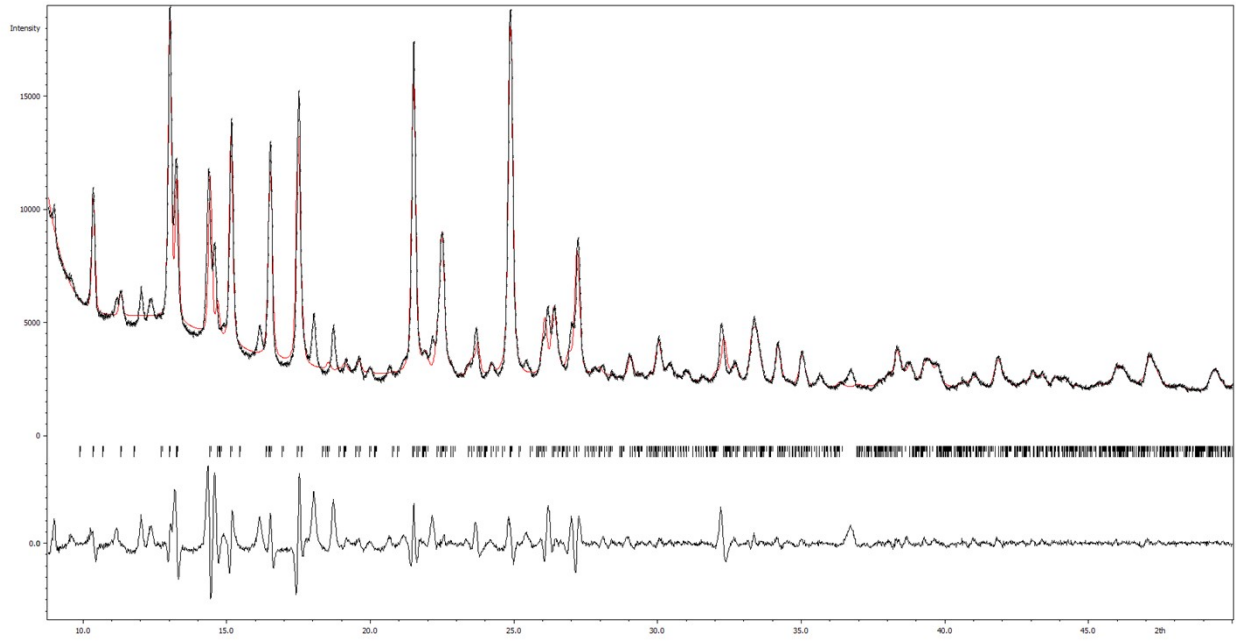

Figure S29. Experimental (black) and simulated (red) X-ray powder diffraction patterns of **Rh2**.

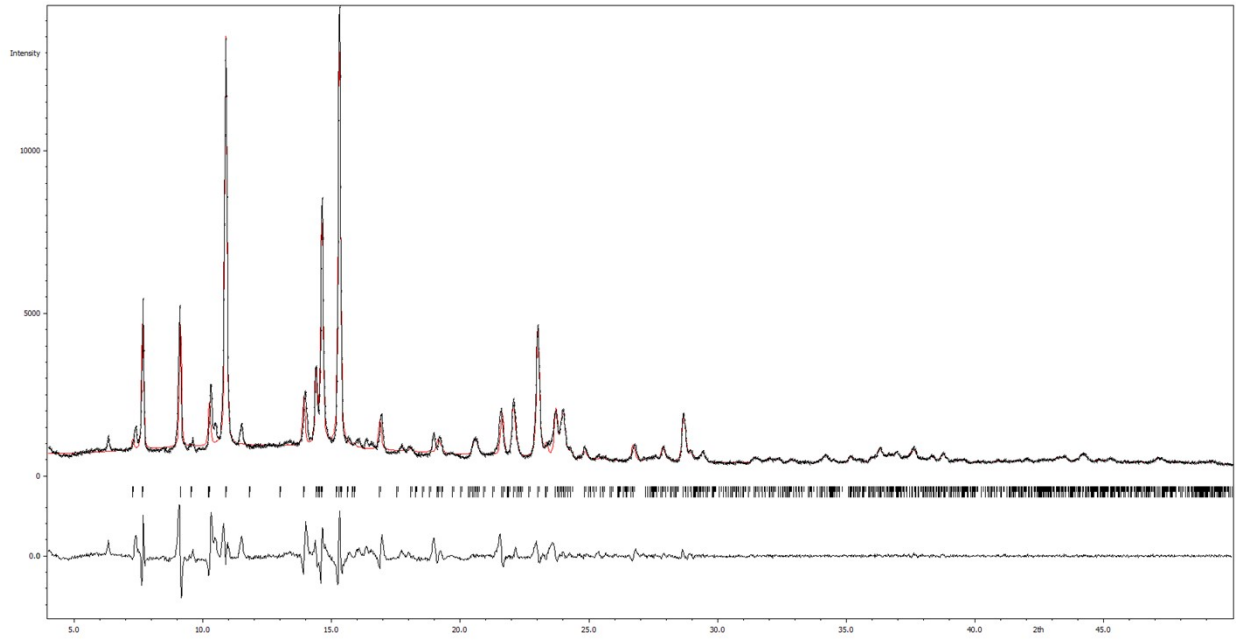

Figure S30. Experimental (black) and simulated (red) X-ray powder diffraction patterns of **Rh3**.

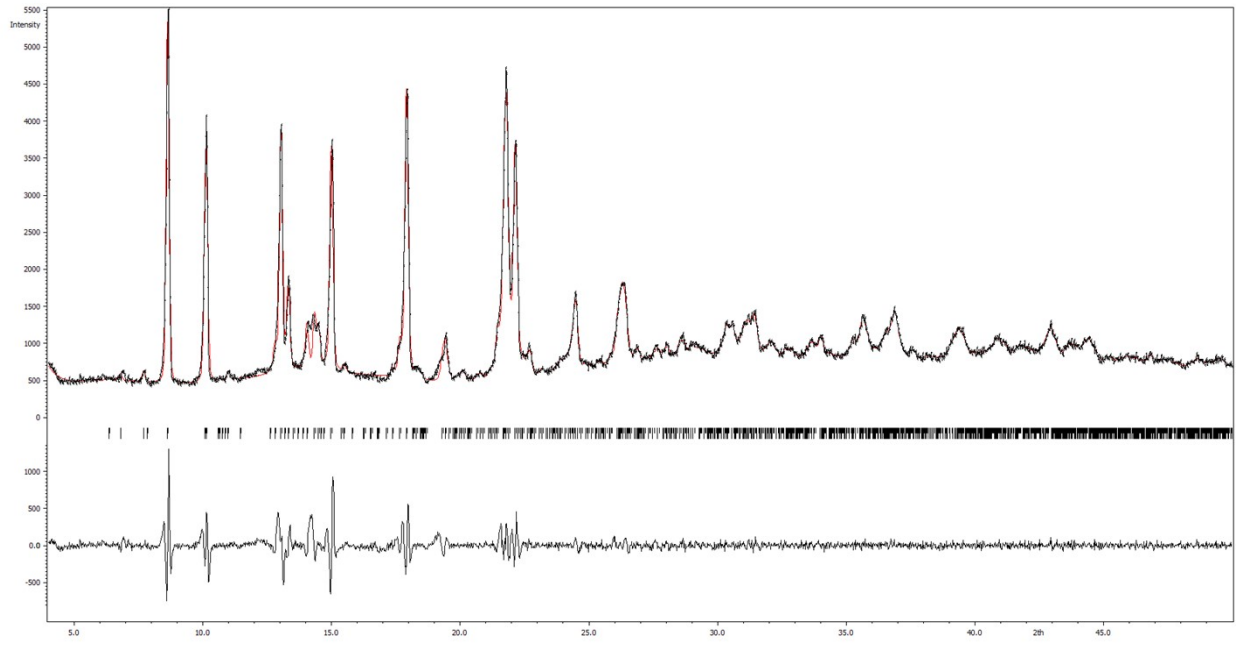

Figure S31. Experimental (black) and simulated (red) X-ray powder diffraction patterns of **Rh4**.

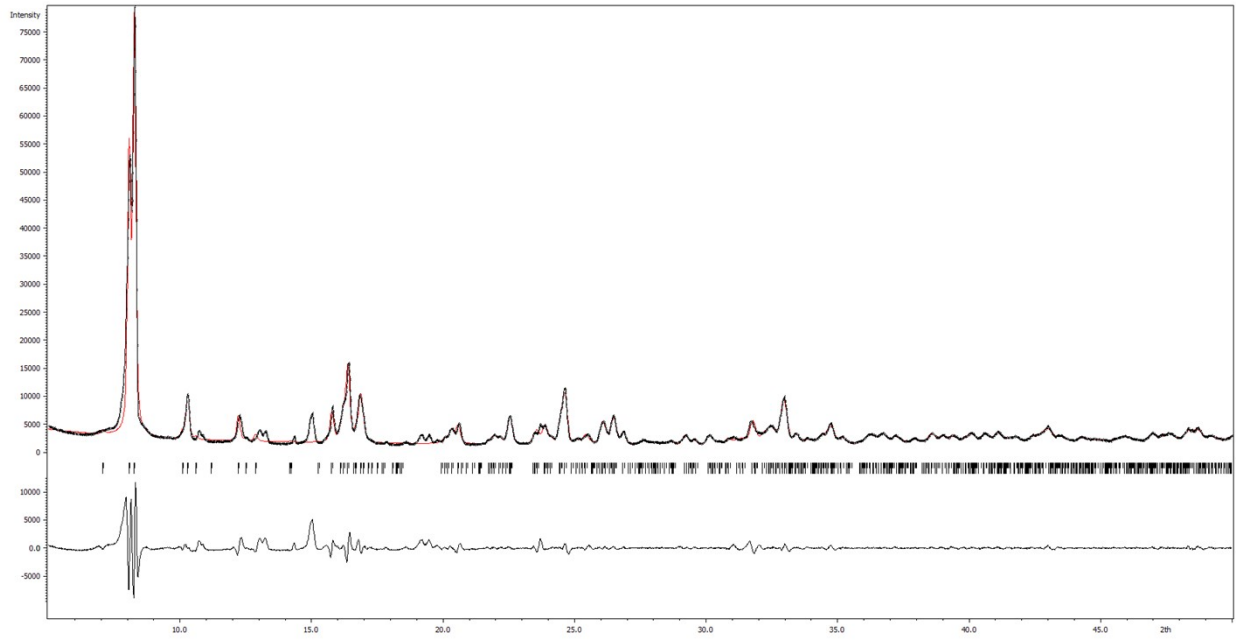

Figure S32. Experimental (black) and simulated (red) X-ray powder diffraction patterns of **Ir1**.

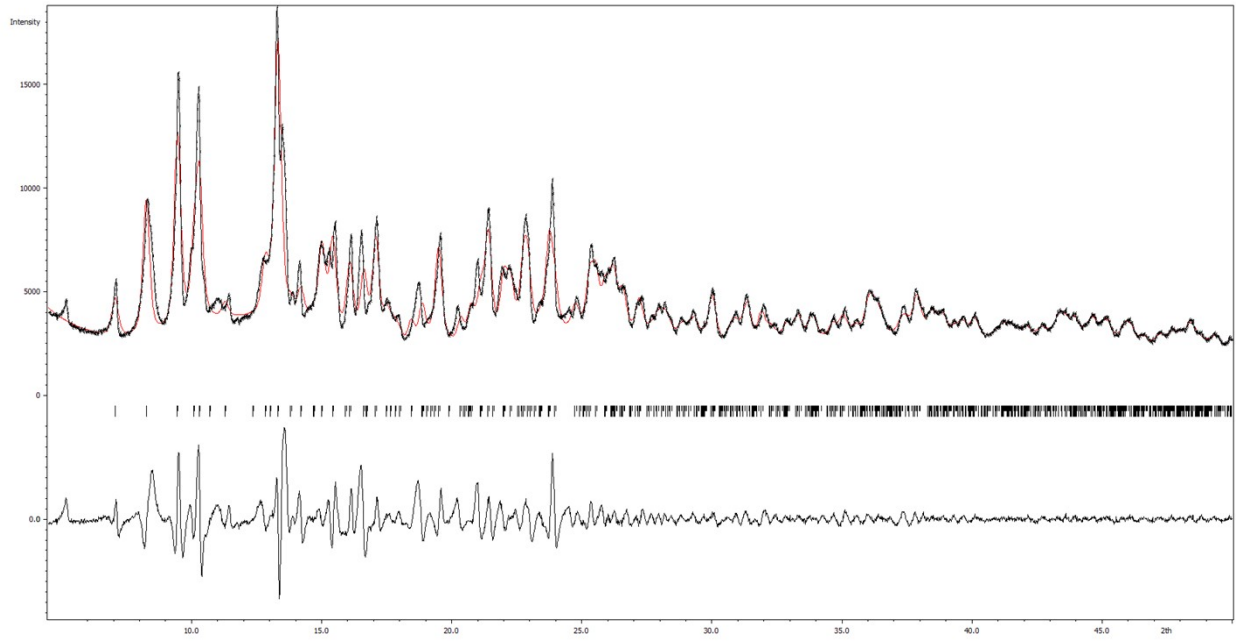

Figure S33. Experimental (black) and simulated (red) X-ray powder diffraction patterns of **Ir2**.

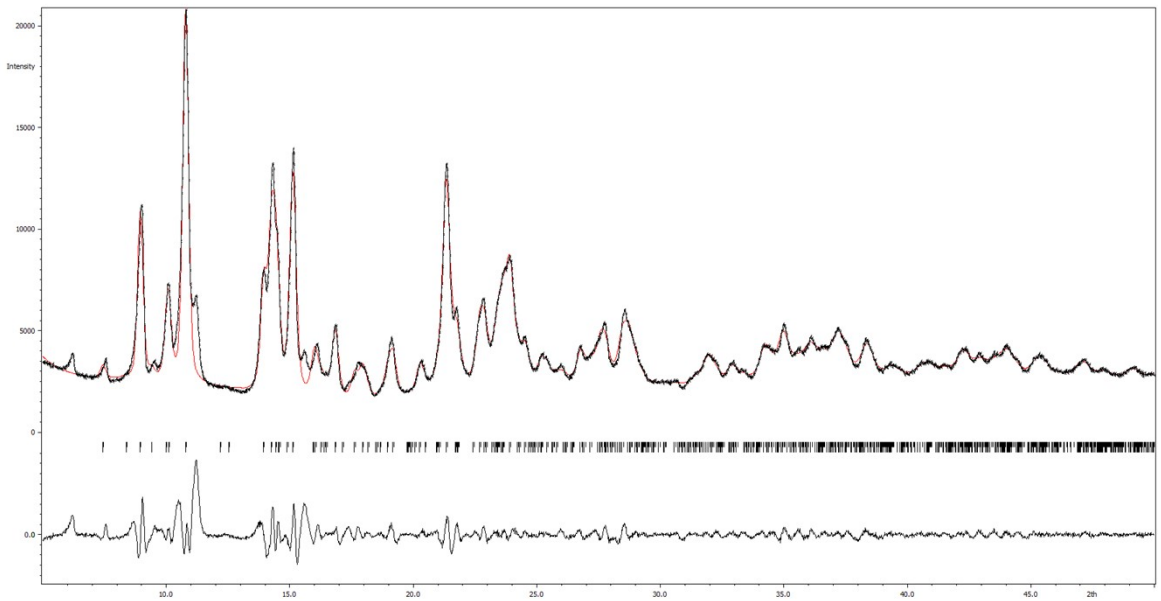

Figure S34. Experimental (black) and simulated (red) X-ray powder diffraction patterns of **Ir3**.

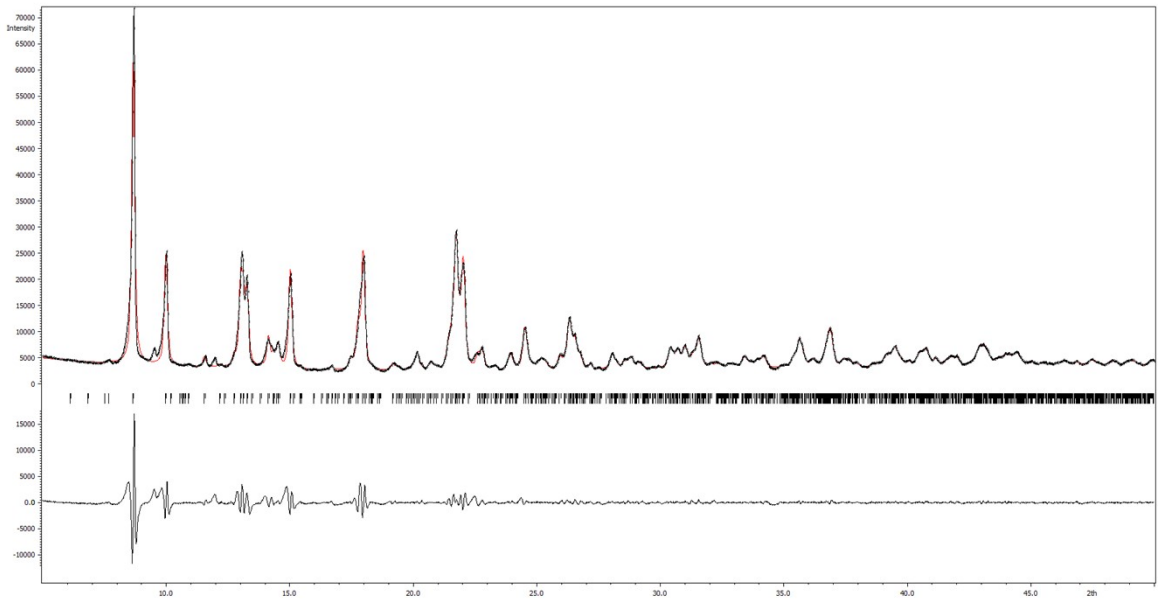

Figure S35. Experimental (black) and simulated (red) X-ray powder diffraction patterns of **Ir4.**

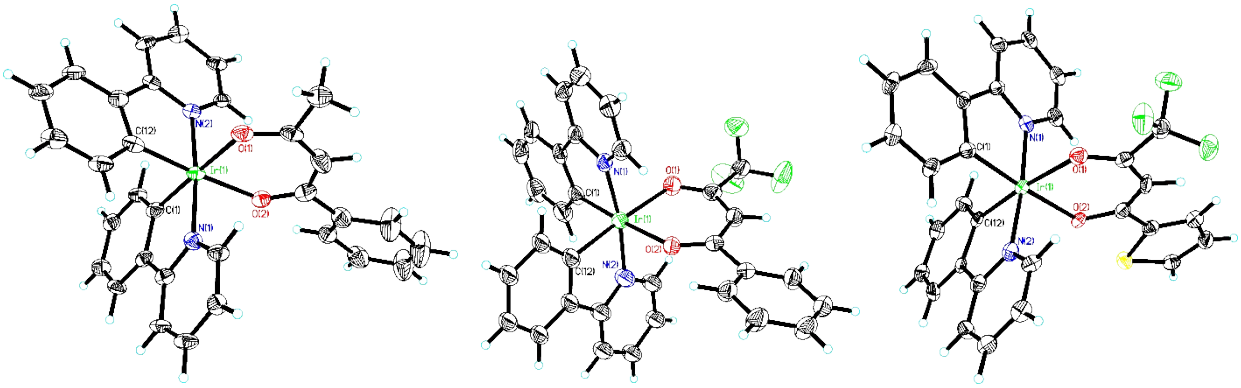

Figure S36. Molecular structures of **Ir2**, **Ir3**, **Ir4**. Displacement ellipsoids are drawn at 50% probability level.

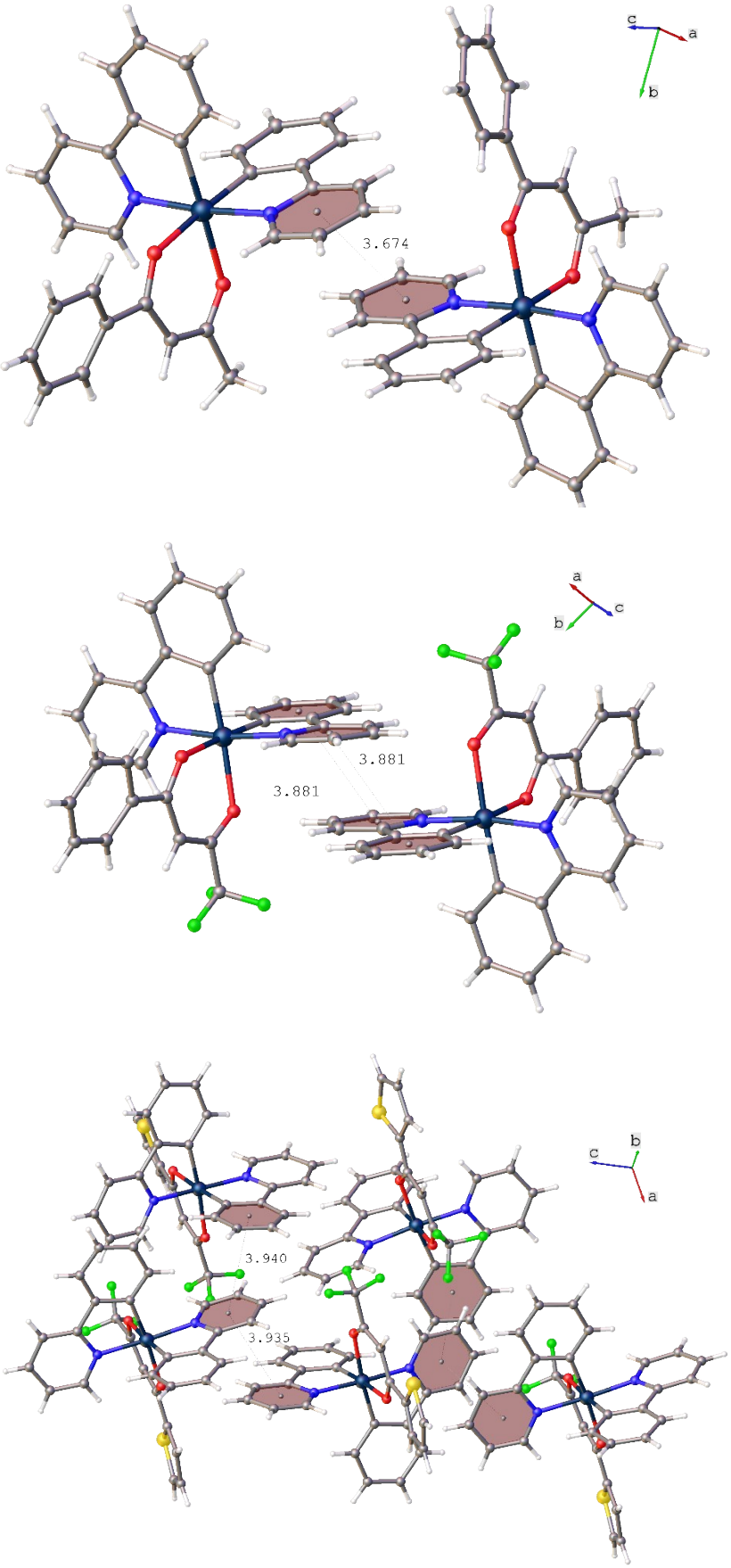

Figure S37. π-π interactions in complexes **Ir2**, **Ir3**, **Ir4**. Centroid-centroid distances are presented in Å.

4. Spectroscopic study

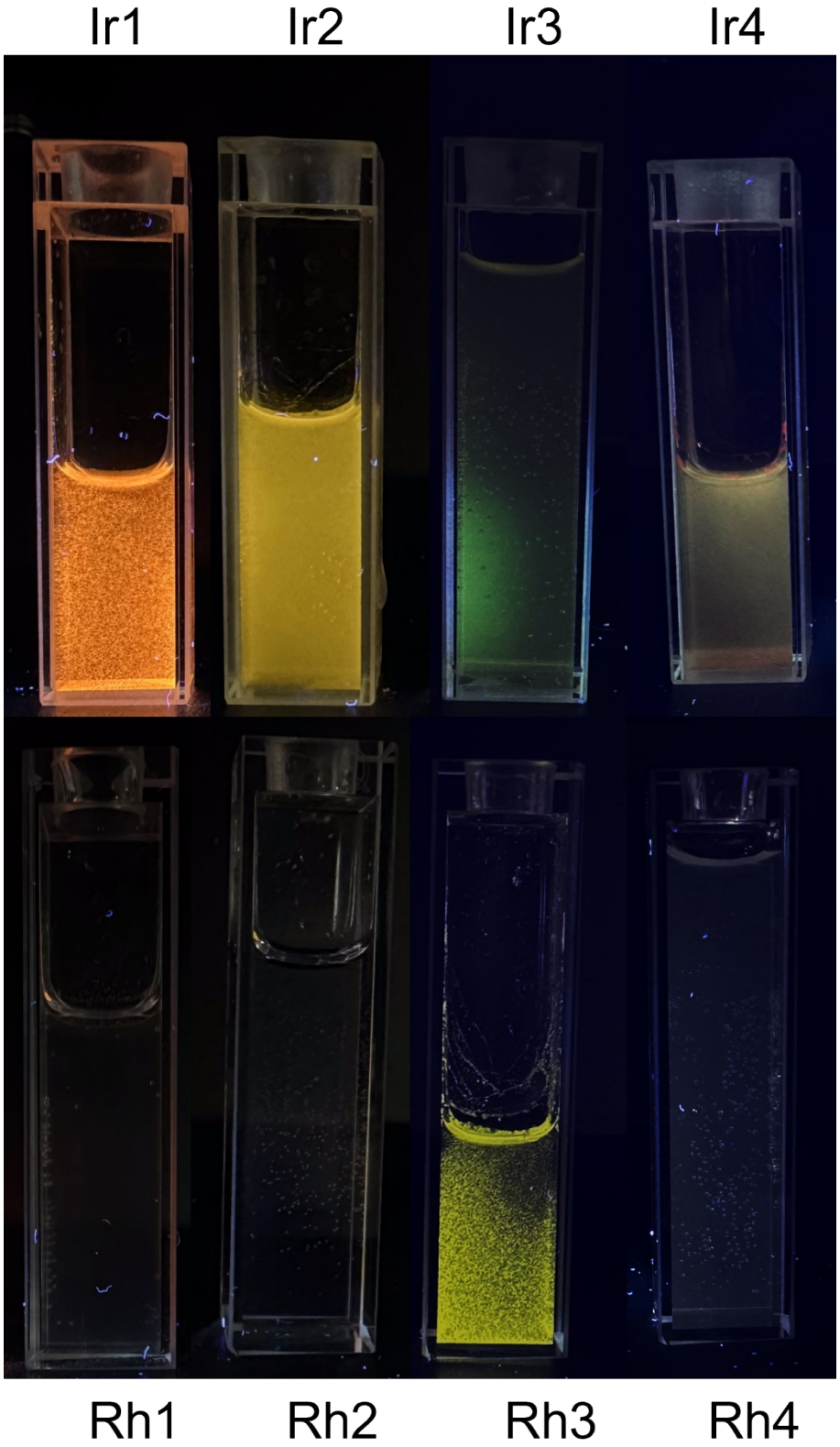

Figure S38. Luminescence photographs of **Rh1** – **Rh4** and **Ir1** – **Ir4** in CH_3CN/H_2O (1/3) solution at 298 K (λ_{ex} = 365 nm).

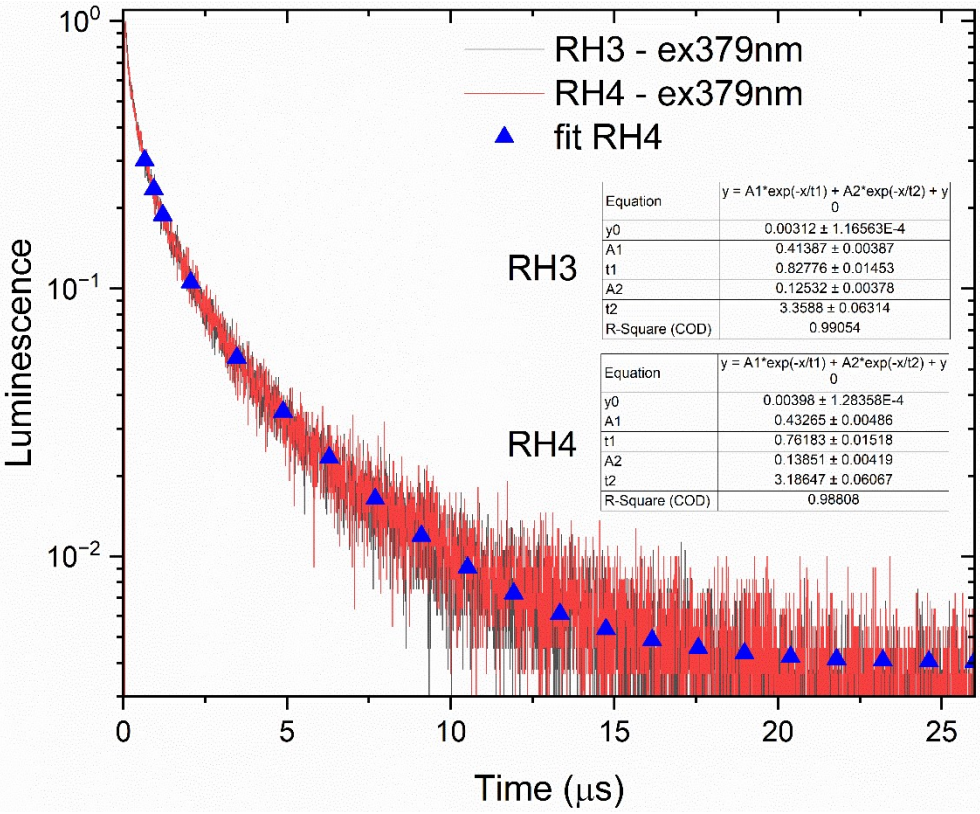

Equation	y = A1*exp(-x/t1) + A2*exp(-x/t2) + y0
y0	0.00312 ± 1.16563E-4
A1	0.41387 ± 0.00387
t1	0.82776 ± 0.01453
A2	0.12532 ± 0.00378
t2	3.3588 ± 0.06314
R-Square (COD)	0.99054

Equation	y = A1*exp(-x/t1) + A2*exp(-x/t2) + y0
y0	0.00398 ± 1.28358E-4
A1	0.43265 ± 0.00486
t1	0.76183 ± 0.01518
A2	0.13851 ± 0.00419
t2	3.18647 ± 0.06067
R-Square (COD)	0.98808

Figure S39. Luminescence decay of **Rh3** – **Rh4** in solid state at 298 K (λ_{ex} = 379 nm).

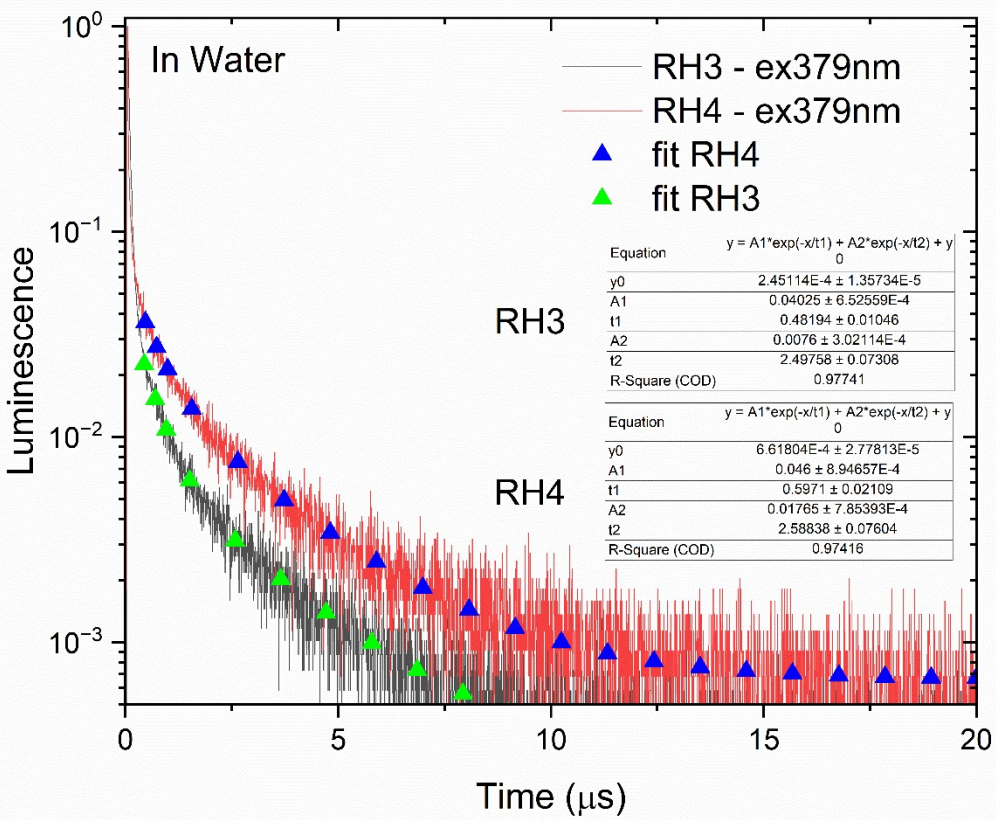

Equation	y = A1*exp(-x/t1) + A2*exp(-x/t2) + y0
y0	2.45114E-4 ± 1.35734E-5
A1	0.04025 ± 6.52559E-4
t1	0.48194 ± 0.01046
A2	0.0076 ± 3.02114E-4
t2	2.49758 ± 0.07308
R-Square (COD)	0.97741

Equation	y = A1*exp(-x/t1) + A2*exp(-x/t2) + y0
y0	6.61804E-4 ± 2.77813E-5
A1	0.046 ± 8.94657E-4
t1	0.5971 ± 0.02109
A2	0.01765 ± 7.85393E-4
t2	2.58838 ± 0.07604
R-Square (COD)	0.97416

Figure S40. Luminescence decay of **Rh3** – **Rh4** in CH_3CN/H_2O (1/3) solution at 298 K (λ_{ex} = 379 nm).

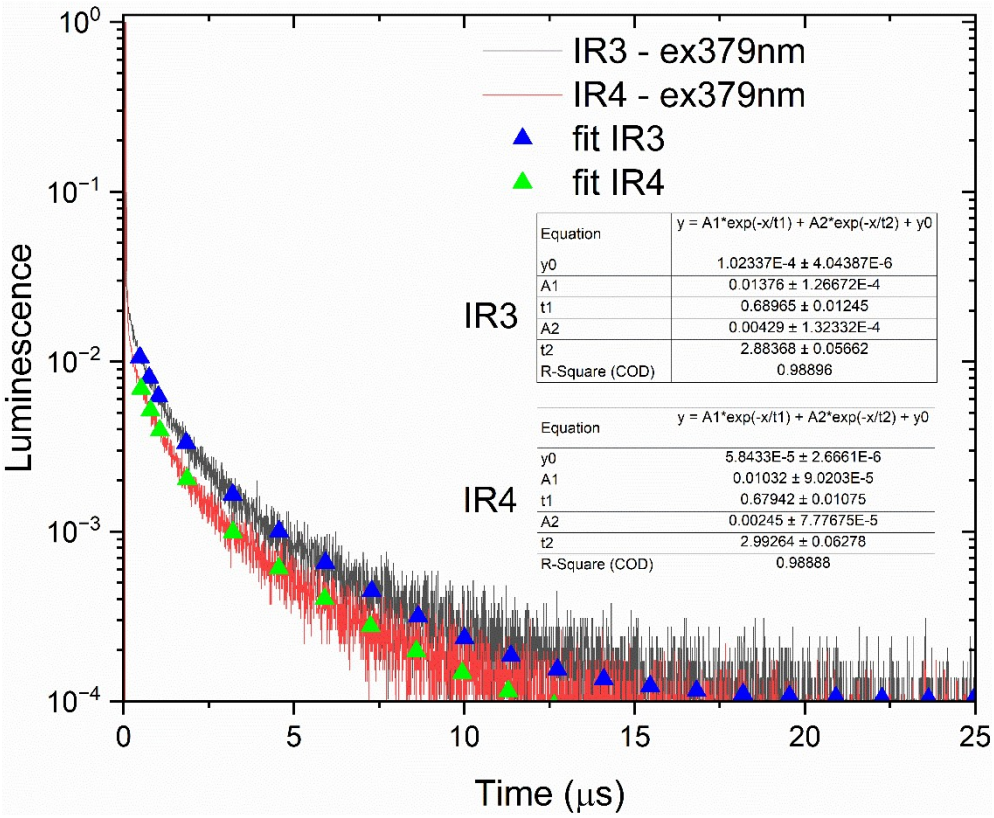

Figure S41. Luminescence decay of **Ir3** – **Ir4** in solid state at 298 K (λ_{ex} = 379 nm).

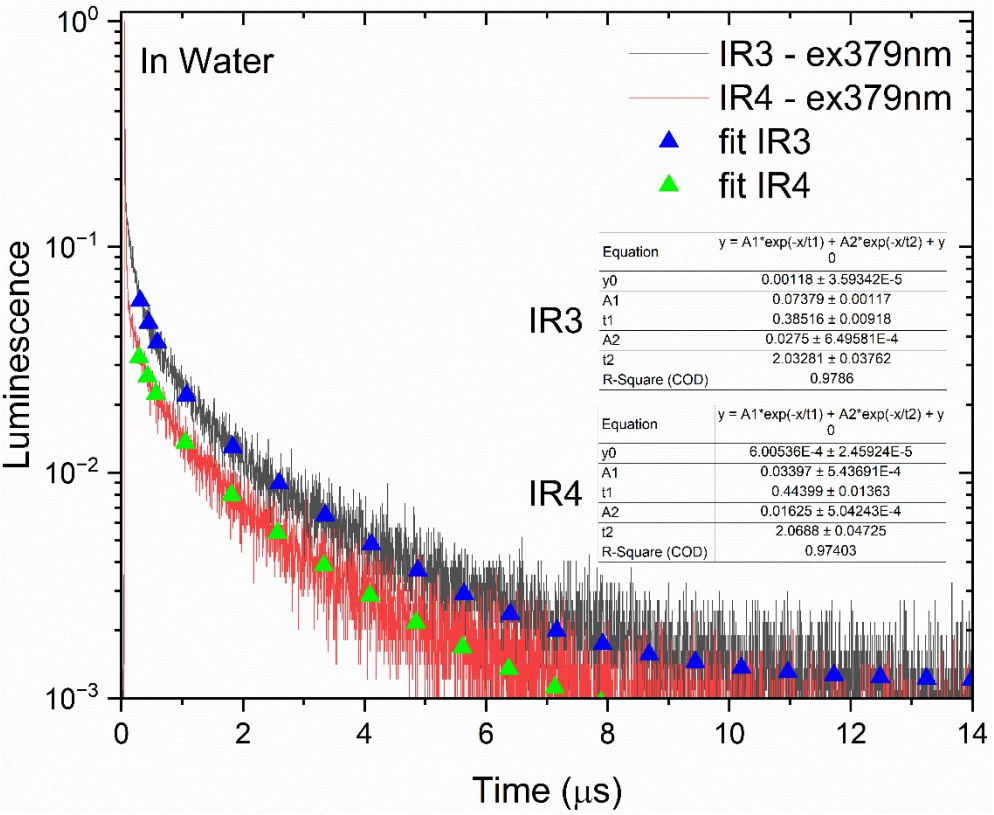

Figure S42. Luminescence decay of **Ir3** – **Ir4** in CH_3CN/H_2O (1/3) solution at 298 K (λ_{ex} = 379 nm).

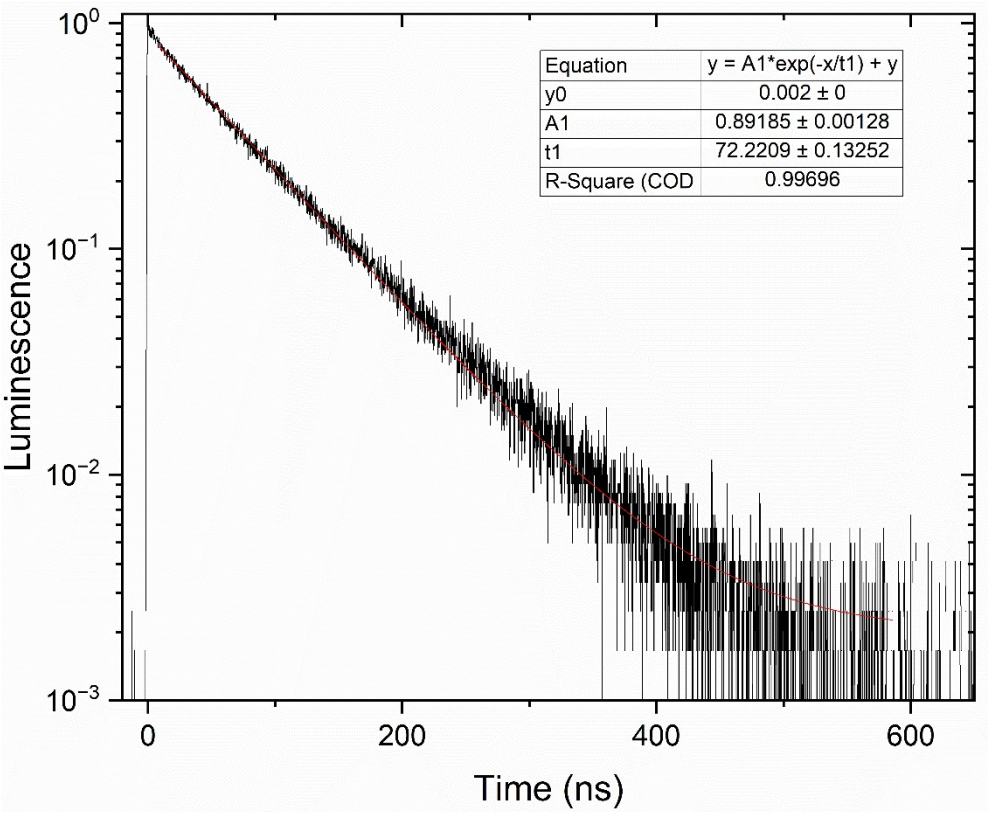

Figure S43. Luminescence decay of solid **Ir1** at 298 K (λ_{ex} = 376 nm).

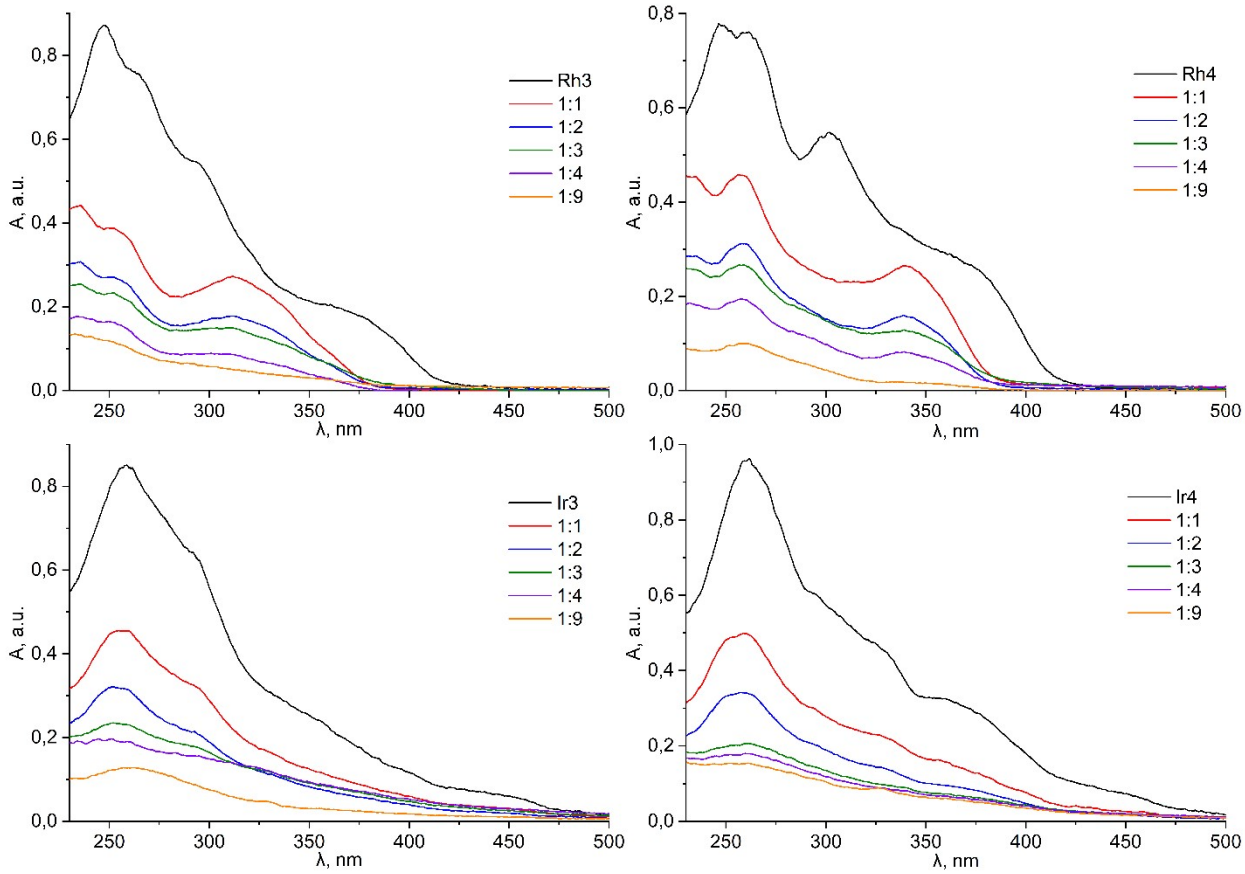

Figure S44. Absorption spectra of **Rh3** – **Rh4** and **Ir3** – **Ir4** in CH_3CN upon increasing the volume ratio of water from 1:1 to 1:9.

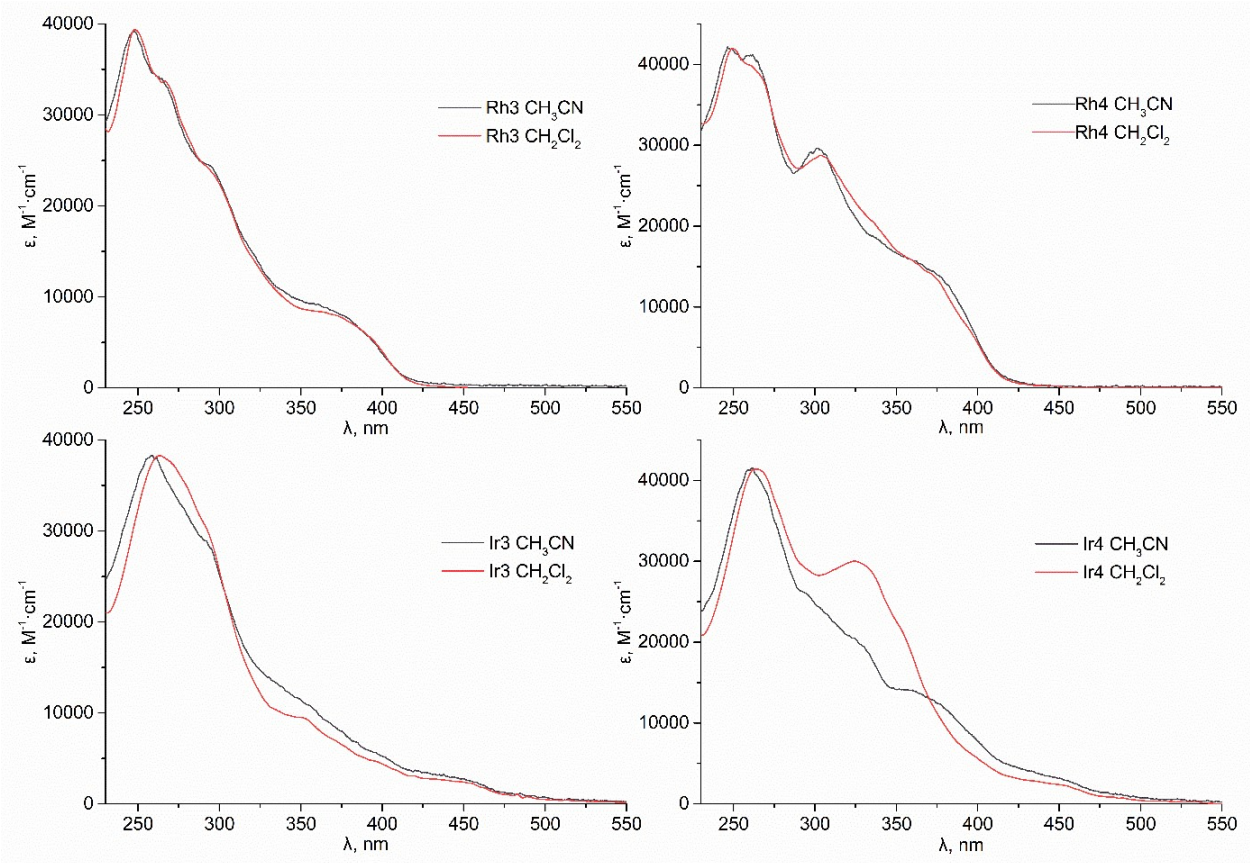

Figure S45. Absorption spectra of **Rh3** – **Rh4** and **Ir3** – **Ir4** in CH_3CN (black) and CH_2Cl_2 (red).

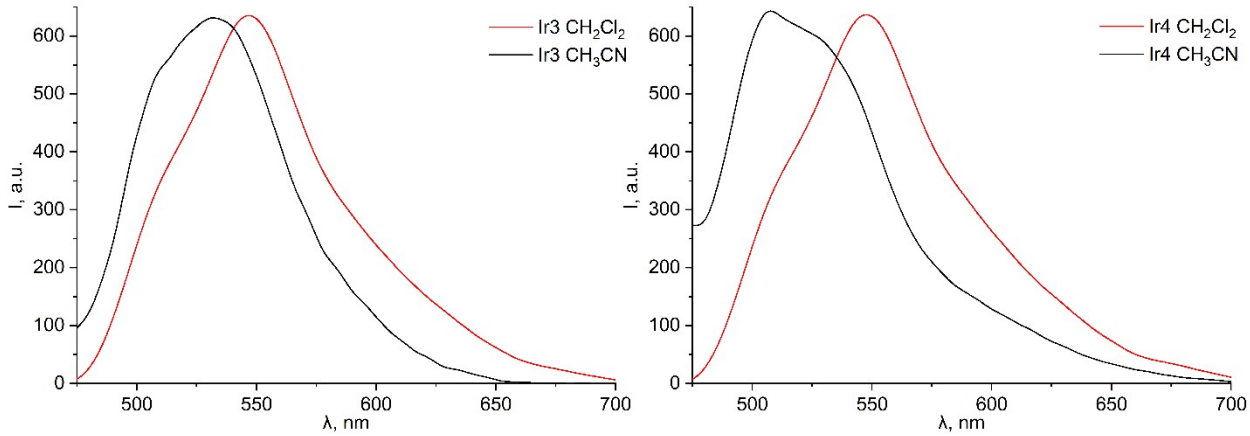

Figure S46. Luminescence spectra of **Ir3** – **Ir4** in CH_3CN (black) and CH_2Cl_2 (red).

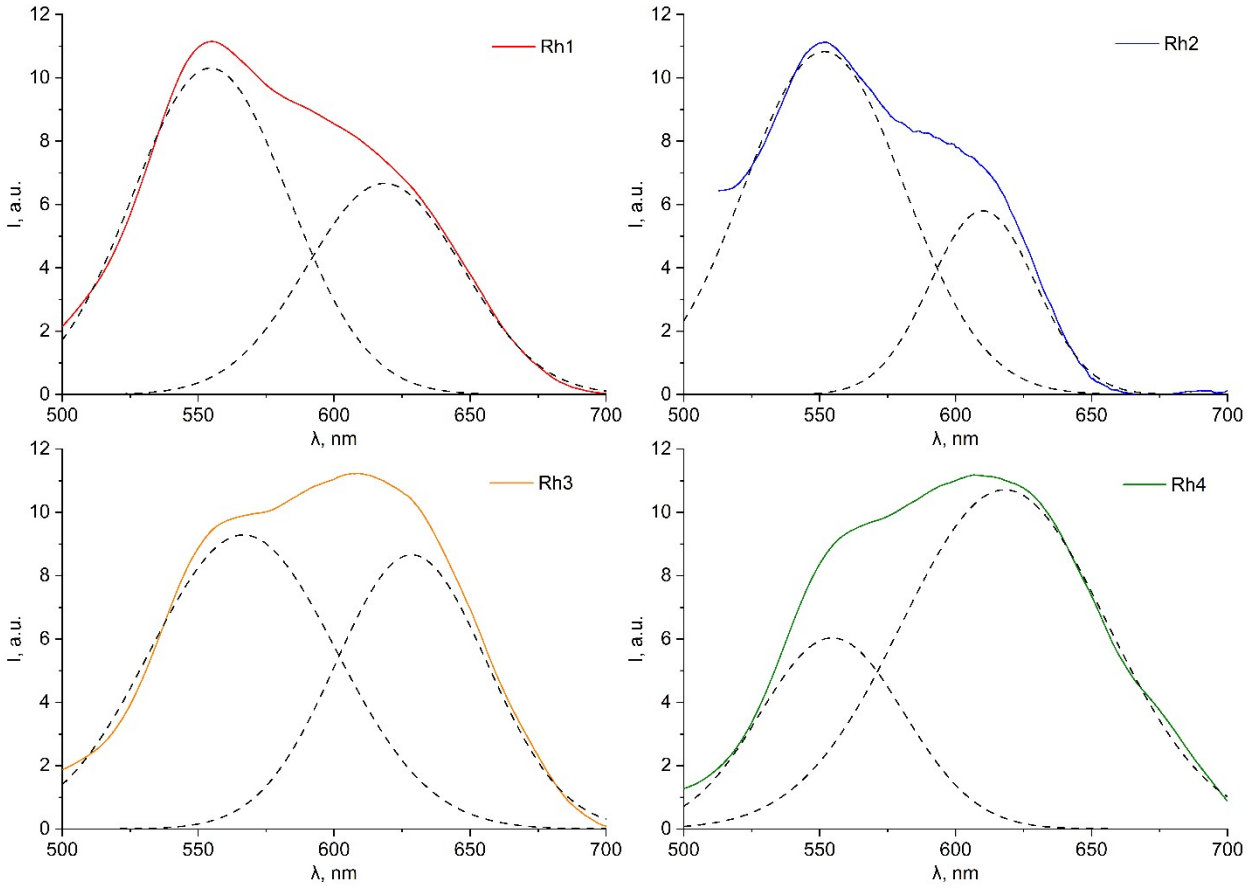

Figure S47. Luminescence spectra of **Rh1** – **Rh4** decomposed into their Gaussian components.

5. *Computational details*

Density functional theory (DFT) calculations were performed with Firefly QC package [9], which is partially based on the GAMESS (US) [10] source code, using the B3LYP functional [11], Stuttgart-Dresden effective core potentials (ECP) for iridium and rhodium and def2-svp basis sets for all other atoms [12, 13]. Frequency analysis was carried out to check if optimized structures were local minima. No imaginary frequencies were found for local minima. Time-dependent DFT (TDDFT) calculations were carried out at the ground state geometries to obtain vertical excitation energies and theoretical absorption spectra. The lowest 30 singlet-singlet excitations were computed. Triplet geometries were calculated using the unrestricted B3LYP method (UB3LYP). Then, single point calculations were performed at the optimized triplet geometry with spin multiplicity 1. The emission energies were calculated by the difference $E(T_1) – E(S_0$ in the geometry of T_1). TDDFT calculations on the optimized triplet geometry with spin multiplicity 1 were performed to obtain energies of the T_2 states. This methodology is proved to provide good estimates of emission energies and emission orbital characteristics [14-16].

Table S4. Selected bond lengths in optimized structures of **Rh1** – **Ir4** at the ground state.

	Rh1	**Rh2**	**Rh3**	**Rh4**	**Ir1**	**Ir2**	**Ir3**	**Ir4**
M – C1	1.9919	1.9928	1.9905	1.9904	2.0050	2.0056	2.0040	2.0040
M – C2	1.9938	1.9936	1.9906	1.9909	2.0059	2.0053	2.0039	2.0040
M – N1	2.0567	2.0545	2.0575	2.0560	2.0552	2.0552	2.0565	2.0555
M – N2	2.0548	2.0558	2.0562	2.0572	2.0547	2.0546	2.0566	2.0565
M – O1	2.1776	2.1806	2.1812	2.2021	2.1621	2.1687	2.1791	2.1833
M – O2	2.1746	2.1785	2.1992	2.1841	2.1629	2.1661	2.1668	2.1690

Table S5. Composition (%) of frontier molecular orbitals for **Rh1** – **Ir4**.

complex		**Rh1**	**Rh2**	**Rh3**	**Rh4**	**Ir1**	**Ir2**	**Ir3**	**Ir4**
HOMO	M	60	61	59	52	60	61	59	52
	ppy	32	32	35	42	33	32	35	41
	O^O	8	7	6	6	7	7	6	7
	energy, eV	–5.37	–5.34	–5.52	–5.52	–4.98	–4.96	–5.15	–5.15
LUMO	M	2	4	2	3	4	3	4	5
	ppy	15	95	14	12	13	45	14	12
	O^O	83	1	84	85	83	52	82	83
	energy, eV	–1.65	–1.56	–1.82	–1.92	–1.81	–1.56	–2.00	–2.09

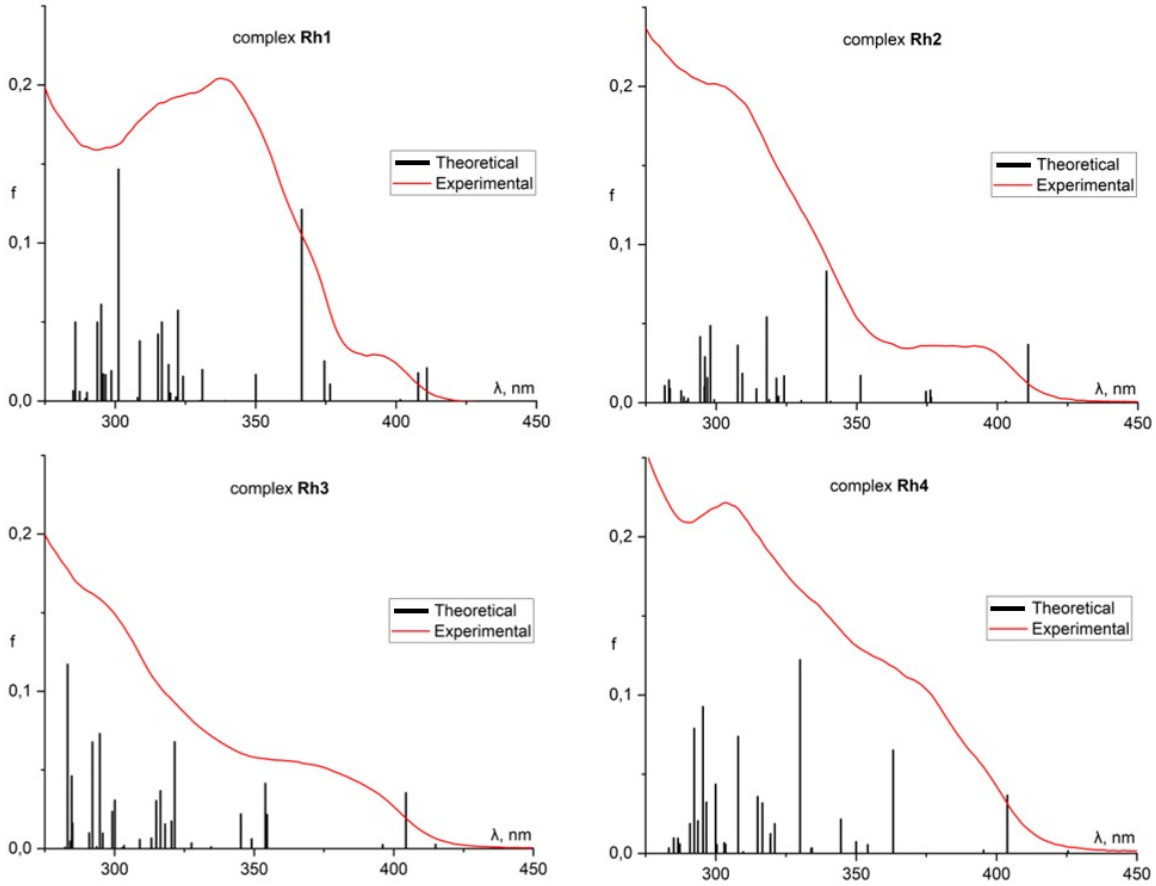

Figure S48. Experimental and TDDFT electronic spectra of **Rh1** – **Rh4**.

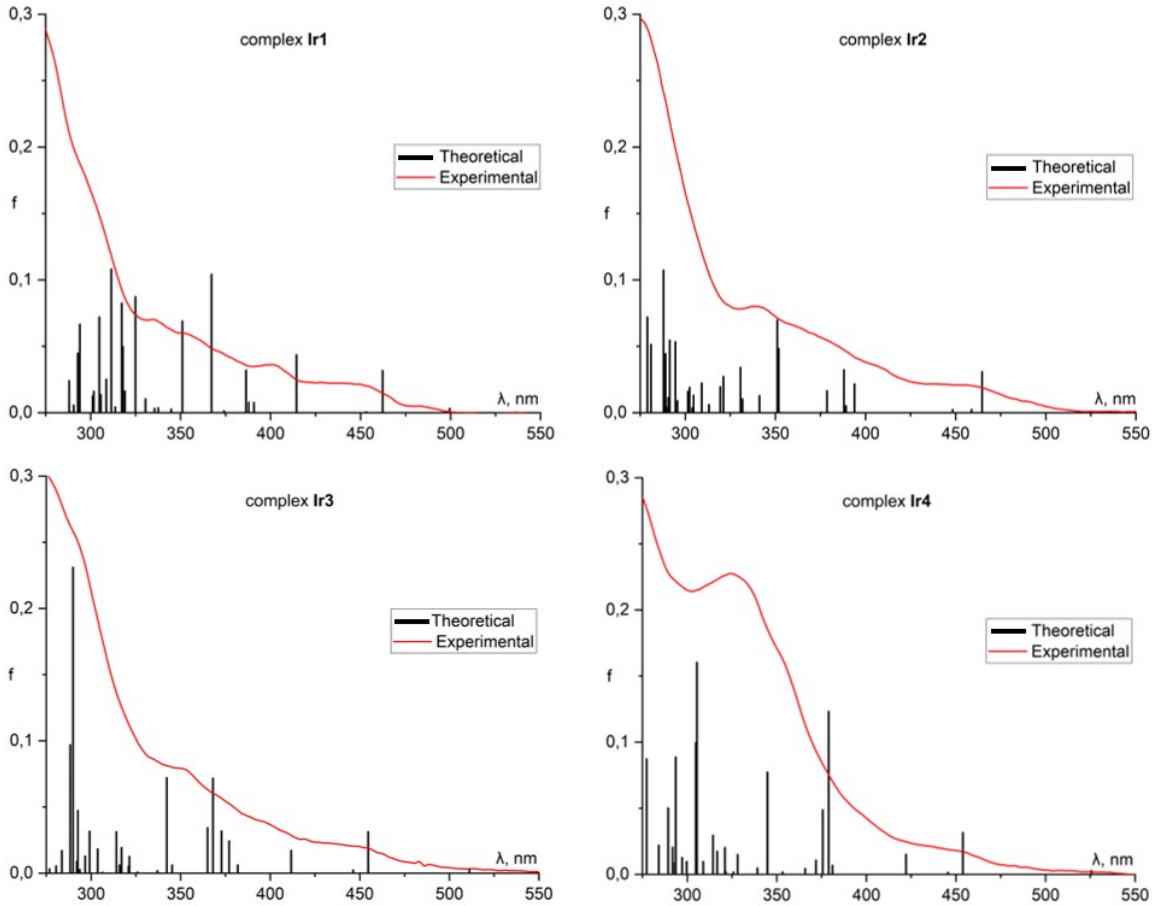

Figure S49. Experimental and TDDFT electronic spectra of **Ir1** – **Ir4**.

Table S6. TDDFT singlet excited states for **Rh1** – **Rh4**.

Complex	State	λ / nm (f)	Dominant monoexcitations
Rh1	S1	410 (0.021)	H → L (54%) {*d(Rh) → π*(O^O), π(ppy) → π*(O^O)*} H → L+1 (42%) {*d(Rh) → π*(ppy), π(ppy) → π*(ppy)*}
	S2	408 (0.018)	H → L+1 (51%) {*d(Rh) → π*(ppy), π(ppy) → π*(ppy)*} H → L (44%) {*d(Rh) → π*(O^O), π(ppy) → π*(O^O)*}
	S4	377 (0.011)	H-1 → L+1 (66%) {*d(Rh) → π*(ppy), π(O^O) → π*(ppy)*} H-1 → L+2 (26%) {*d(Rh) → π*(ppy), π(O^O) → π*(ppy)*}
	S5	374 (0.025)	H-1 → L+2 (48%) {*d(Rh) → π*(ppy), π(O^O) → π*(ppy)*} H-1 → L+1 (25%) {*d(Rh) → π*(ppy), π(O^O) → π*(ppy)*} H-1 → L (22%) {*d(Rh) → π*(O^O), π(O^O) → π*(O^O)*}
	S6	366 (0.121)	H-1 → L (69%) {*d(Rh) → π*(O^O), π(O^O) → π*(O^O)*} H-1 → L+2 (21%) {*d(Rh) → π*(ppy), π(O^O) → π*(ppy)*}
Rh2	S1	411 (0.037)	H → L (94%) {*d(Rh) → π*(ppy), π(ppy) → π*(ppy)*}
	S4	376 (0.008)	H-1 → L (38%) {*d(Rh) → π*(ppy), π(O^O) → π*(ppy)*} H-1 → L+1 (31%) {*d(Rh) → π*(ppy), π(O^O) → π*(ppy)*} H → L+2 (27%) {*d(Rh) → π*(O^O), π(ppy) → π*(O^O)*}
	S5	375 (0.007)	H-1 → L+1 (58%) {*d(Rh) → π*(ppy), π(O^O) → π*(ppy)*} H-1 → L (36%) {*d(Rh) → π*(ppy), π(O^O) → π*(ppy)*}
	S6	351 (0.017)	H → L+3 (96%) {*d(Rh) → π*(ppy), π(ppy) → π*(ppy)*}
	S8	339 (0.083)	H-1 → L+2 (86%) {*d(Rh) → π*(O^O), π(O^O) → π*(O^O)*}
Rh3	S1	415 (0.003)	H → L (96%) {*d(Rh) → π*(O^O), π(ppy) → π*(O^O)*}
	S2	404 (0.036)	H → L+1 (90%) {*d(Rh) → π*(ppy), π(ppy) → π*(ppy)*}
	S3	396 (0.003)	H → L+2 (93%) {*d(Rh) → π*(ppy), π(ppy) → π*(ppy)*}
	S4	355 (0.022)	H-1 → L+1 (50%) {*d(Rh) → π*(ppy), π(O^O) → π*(ppy)*} H-1 → L+2 (26%) {*d(Rh) → π*(ppy), π(O^O) → π*(ppy)*} H-1 → L (15%) {*d(Rh) → π*(O^O), π(O^O) → π*(O^O)*}
	S5	354 (0.041)	H-1 → L (57%) {*d(Rh) → π*(O^O), π(O^O) → π*(O^O)*} H-1 → L+1 (30%) {*d(Rh) → π*(ppy), π(O^O) → π*(ppy)*}
Rh4	S1	425 (0.0015)	H → L (98%) {*d(Rh) → π*(O^O), π(ppy) → π*(O^O)*}
	S2	404 (0.037)	H → L+1 (93%) {*d(Rh) → π*(ppy), π(ppy) → π*(ppy)*}
	S4	363 (0.065)	H-1 → L (87%) {*d(Rh) → π*(O^O), π(O^O) → π*(O^O)*}
	S7	345 (0.022)	H → L+3 (93%) {*d(Rh) → π*(ppy), π(ppy) → π*(ppy)*}
	S10	330 (0.122)	H-3 → L (73%) {*d(Rh) → π*(O^O), π(ppy) → π*(O^O)*} H-2 → L (5%) {*π(ppy) → π*(O^O)*}

Table S7. TDDFT singlet excited states for **Ir1** – **Ir4**.

Ir1	S1	500 (0.003)	H → L (99%) {*d(Ir) → π*(O^O), π(ppy) → π*(O^O)*}
	S2	462 (0.032)	H → L+1 (95%) {*d(Ir) → π*(ppy), π(ppy) → π*(ppy)*}
	S4	414 (0.044)	H-1 → L (95%) {*d(Ir) → π*(O^O), π(O^O) → π*(O^O)*}
	S7	386 (0.032)	H → L+3 (67%) {*d(Ir) → π*(ppy), π(ppy) → π*(ppy)*} H-1 → L+2 (27%) {{*d(Ir) → π*(ppy), π(O^O) → π*(ppy)*}
	S9	367 (0.104)	H-2 → L (89%) {*d(Ir) → π*(O^O)*} H-2 → L+2 (8%) {*d(Ir) → π*(ppy)*}
Ir2	S1	465 (0.031)	H → L+1 (80%) {*d(Ir) → π*(ppy), π(ppy) → π*(ppy)*} H → L (17%) {*d(Ir) → π*(O^O), π(ppy) → π*(O^O)*}
	S4	394 (0.022)	H-1 → L (63%) {*d(Ir) → π*(ppy), π(O^O) → π*(O^O)*} H-1 → L+2 (18%) {*d(Ir) → π*(ppy), π(O^O) → π*(O^O)*} H → L+3 (14%) {*d(Ir) → π*(ppy), π(ppy) → π*(ppy)*}
	S6	388 (0.032)	H → L+3 (70%) {*d(Ir) → π*(ppy), π(ppy) → π*(ppy)*} H-1 → L+1 (12%) {*d(Ir) → π*(ppy), π(O^O) → π*(ppy)*} H-1 → L (8%) {*d(Ir) → π*(ppy), π(O^O) → π*(O^O)*}
	S9	352 (0.048)	H-2 → L (84%) {*d(Ir) → π*(ppy), d(Ir) → π*(O^O)*} H-2 → L+2 (6%) {*d(Ir) → π*(ppy), d(Ir) → π*(O^O)}*
	S10	351 (0.070)	H-2 → L+1 (86%) {*d(Ir) → π*(ppy)*} H-1 → L+2 (6%) {*d(Ir) → π*(ppy), π(O^O) → π*(O^O)*}
Ir3	S1	511 (0.003)	H → L (99%) {*d(Ir) → π*(O^O), π(ppy) → π*(O^O)*}
	S2	455 (0.031)	H → L+1 (91%) {*d(Ir) → π*(ppy), π(ppy) → π*(ppy)*}
	S4	412 (0.017)	H-1 → L (96%) {*d(Ir) → π*(O^O), π(O^O) → π*(O^O)*}
	S8	368 (0.072)	H-2 → L (48%) {*d(Ir) → π*(O^O)*} H → L+4 (43%) {*d(Ir) → π*(ppy), π(ppy) → π*(ppy)*}
	S9	365 (0.034)	H-2 → L (37%) {*d(Ir) → π*(O^O)*} H → L+4 (21%) {*d(Ir) → π*(ppy), π(ppy) → π*(ppy)*} H-1 → L+2 (14%) {*d(Ir) → π*(ppy), π(O^O) → π*(ppy)*} H-1 → L+1 (12%) {*d(Ir) → π*(ppy), π(O^O) → π*(ppy)*} H-2 → L+2 (12%) {*d(Ir) → π*(ppy)*}
Ir4	S1	526 (0.003)	H → L (98%) {*d(Ir) → π*(O^O), π(ppy) → π*(O^O)*}
	S2	454 (0.032)	H → L+1 (93%) {*d(Ir) → π*(ppy), π(ppy) → π*(ppy)*}
	S6	379 (0.123)	H-2 → L (67%) {*d(Ir) → π*(O^O)*} H-1 → L+1 (24%) *{d(Ir) → π*(ppy), π(O^O) → π*(ppy)}*
	S7	376 (0.049)	H-1 → L+1 (34%) {*d(Ir) → π*(ppy), π(O^O) → π*(ppy)*} H-1 → L+2 (33%) {*d(Ir) → π*(ppy), π(O^O) → π*(ppy)*} H-2 → L (16%) {*d(Ir) → π*(O^O)*} H → L+3 (6%) {*d(Ir) → π*(ppy), π(ppy) → π*(ppy)*} H-2 → L+1 (6%) {*d(Ir) → π*(ppy)*}
	S11	345 (0.077)	H-2 → L+1 (64%) {*d(Ir) → π*(ppy)*} H-2 → L+2 (20%) {*d(Ir) → π*(ppy)*} H-1 → L+2 (9%) {*d(Ir) → π*(ppy), π(O^O) → π*(ppy)*}

Table S8. Spin density distribution (%) for complexes **Rh1** – **Rh4**, **Ir1** – **Ir4** at their T_1 states.

complex		**Rh1**	**Rh2**	**Rh3**	**Rh4**	**Ir1**	**Ir2**	**Ir3**	**Ir4**
moiety	M	3	7	11	10	16	18	19	20
	O^O	96	92	88	89	71	68	64	61
	C^N	1	1	1	1	13	14	17	19

Table S9. Experimental and calculated emission wavelength for complexes **Rh1** – **Rh4** from the triplet excited state (calculated as l=hc/DE, where DE is $E(T_1)$-$E(S_0$ in T_1 geometry) or $E(T_2)$-$E(S_0$ in T_1 geometry)).

complex	λ_{exp}, nm		λ_{theor}, nm	
Rh1	555	619	457	566
Rh2	552	610	482	566
Rh3	567	628	550	602
Rh4	555	618	544	589

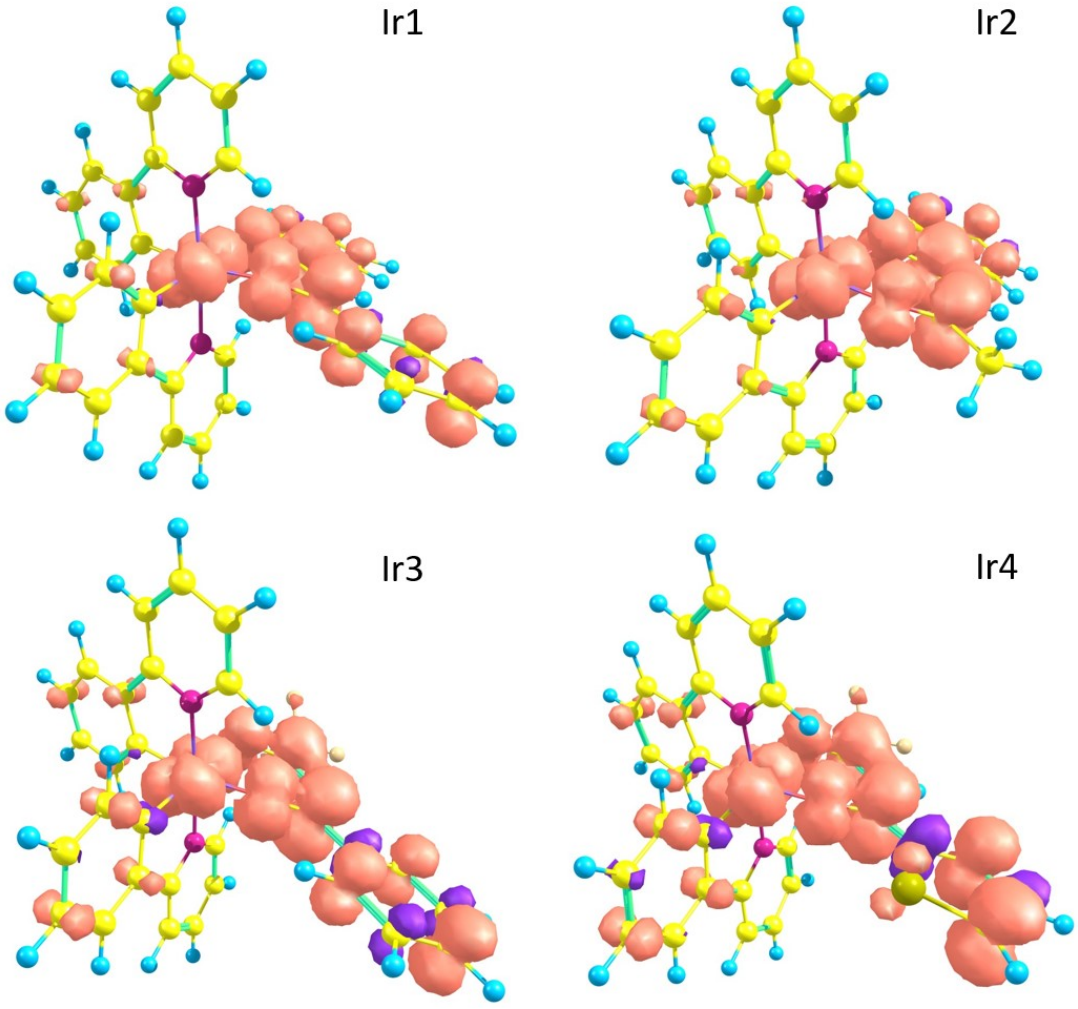

Figure S50. Spin density distribution (SDD) of the lowest triplet excited states (T_1) in complexes **Ir1** – **Ir4**.

References:

1. M. S. Wrighton, D. S. Ginley and D. L. Morse, J. Phys. Chem., 1974, 78, 2229–2233.

2. J. C. De Mello, H. F. Wittmann and R. H. Friend, Adv. Mater., 1997, 9, 230–232.

3. N. C. Greenham, I. D. W. Samuel, G. R. Hayes, R. T. Phillips, Y. A. R. R. Kessener, S. C. Moratti, A. B. Holmes and R. H. Friend, Chem. Phys. Lett., 1995, 241, 89–96.

4. G.M. Sheldrick, SADABS. Version 2008/1. 2008. Bruker AXS Inc. Germany.

5. G.M. Sheldrick, Acta Cryst., 2015, A71, 3–8.

6. G.M. Sheldrick, Acta Cryst., 2015, C71, 3–8.

7. A.L. Spek, Acta Cryst. 2015, C71, 9–18.

8. O.V. Dolomanov, L.J. Bourhis, R.J. Gildea, J.A.K. Howard, H. Puschmann, J. Appl. Cryst., 2009, 42, 339–341.

9. A.A. Granovsky, Firefly version 7.1.G. http://classic.chem.msu.su/gran/firefly/index.html

10. M.W. Schmidt, K.K. Baldridge, J.A. Boatz, S.T. Elbert, M.S. Gordon, J.H. Jensen, S. Koseki, N. Matsunaga, K.A. Nguyen, S. Su, T.L. Windus, M. Dupius, J.A. Montgomery, J. Comput.Chem., 1993, 14, 1347.

11. P.J. Stephens, F.J. Devlin, C.F. Chabalowski, M.J. Frisch, J. Phys. Chem., 1994, 98, 11623.

12. D. Andrae, U. Haussermann, M. Dolg, H. Stoll, H. Preuss, Theor. Chim. Acta., 1990, 77, 123.

13. R. Krishnan, J.S. Binkley, R. Seeger, J.A. Pople, J. Chem. Phys., 1980, 72, 650.

14. F. D.Angelis, S. Fantacci, N.Evans, C.Klein, S. M.Zakeeruddin, J. E.Moser, K.Kalyana-sundaram, H. J.Bolink, M.Grätzel, M. K.Nazeeruddin, Inorg. Chem. 2007, 46, 5989–6001.

15. P. J. Hay, J. Phys. Chem. A, 2002,106, 8, 1634–1641.

16. S. Urinda, G. Das, A. Pramanik, P. Sarkar, Phys. Chem. Chem. Phys., 2017, 19, 43, 29629–29640.